International Journal of Science and Research (IJSR)
ISSN: 2319-7064
Impact Factor 2025: 7.089

# Geology and Geochemistry of Shale and Quartzite of the Cumbum Formation: Implications for Provenance, Source Area Weathering, Climatic Conditions and Tectonic Settings

**Raghunath Mishra[1], Snigdha Dash[2]**

[1, 2]State Unit: Andhra Pradesh, Geological Survey of India, Hyderabad-500068
Corresponding Author Email: *raghunath.mishra[at]gsi.gov.in,*
Email: *raghumishra.kjr[at]gmail.com*

**Abstract:** ***The Mesoproterozoic Cumbum Formation, composed of shales and quartzite, combines geochemical, mineralogical, and sedimentological analyses to unravel the region's ancient climate and tectonic history. High weathering indices and clay mineralogy point to a warm, humid to semi-arid climate during deposition, while provenance and structural aspects reveal a tectonic history dominated by passive margin development. The shales have high Al2O3, Fe2O3, K2O, TiO2, Ga, La, Nb, Rb, Sc, Sr, Th and Y content more than the quartzites, whereas, quartzites are higher in SiO2, Cu, Hf and Zr than the shales. The shale samples plot on the two triangular diagrams in the relatively more weathered region and in the A–CN–K diagram above the granodiorite and shale suggesting a source which had suffered relatively a high degree of chemical weathering. For the quarzitic samples, La/Sc, Th/Sc, La/Co and Th/Co values are more similar to values for sediments derived from felsic source rocks than to those for mafic source rocks, thus suggesting felsic source rock. Th/U ratios in the quartzites range from 0.83 to 1.45 indicating the quartzites neither suffered intense weathering nor intense recycling. When Th/Sc is plotted on the diagram of Zr/Sc–Th/Sc, the recycled source rocks for the all-quartzite samples from the study area are further supported by their high Zr/Sc ratio. Out of four samples two samples are enriched in zircon due to sedimentary sorting and recycling and the rest two samples fall in between andesitic to felsic magmatism field. On a chondrite-normalised diagram, the studied shales display slightly enriched LREE patterns (average LaN/SmN = 5.27), small negative Eu (average Eu/ Eu* = 0.69) and fairly flat HREE patterns (average GdN /YbN = 0.13) except for Yb which are characteristic of sediments derived from upper continental crust. The chondrite-normalized REE patterns for the studied quartzites are characterized by high light REE/heavy REE (LREE/HREE) ratio (6.79 - 15.52), flat HREE pattern except Yb and pronounced negative Eu anomaly. LREEs are fractionated, (La/Sm)n = 4.98 and the HREE patterns are almost flat, (Gd/ Yb) n= 0.15. This chondrite-normalized pattern is typical of sediments and sedimentary rocks enriched in light REE (LREE), flat heavy REE (HREE) and negative Eu anomaly. The quartzites and shales are mostly of quartzose sedimentary provenance, derived from a cratonic interior or recycled orogen with felsic sources input. The shales and quartzites were deposited in a passive margin setting. Th/U versus Th systematics suggests a high degree of chemical weathering for the Cumbum shales suggesting them to be derived from an older crustal material and a depleted mantle source for the quartzites. The geochemistry of the studied shales suggests their origin to be a combination of felsic volcanic rocks (predominantly) and granitic rocks (to a lesser extent).***

**Keywords:** Cumbum Formation, Geochemistry, provenance, weathering, tectonic setting

## 1. Introduction

The crescent-shaped Cuddapah Basin (CB) spread across 45,000 km$^2$, hosts the thickest of the Purana sequence **(Meijerink et al., 1984; Rao et al., 1987; Kale, 1991).** The EGMB borders the Cuddapah basin in the eastern side and the western margin have a well-marked non-conformity of Cuddapah sediments resting on the Archaean Peninsular Gneissic Complex enclosing greenstone belts of Kadiri, Veligallu and Gadwal. Lack of younger cover renders it as an ideal Proterozoic basin for studying sedimentation patterns, interbedded volcanics, intrusive bodies, basement-cover interactions, structural arrangements, and tectonic evolution. Wide spread facies variation is observed in the western Papaghni, Chitravati (Cheyair) and Nallamalai group in the east **(Rao et al.,1987).** Subsequent studies on sedimentological, stratigraphic, structural, paleontological, and tectonic aspects have contributed to the current knowledge of this basin **(Saha and Tripathy, 2012; Matin, 2015; Chakrabarti et al., 2016)**. This epi-cratonic basin (Fig. 1) has been divided into five sub-basins: Papaghni to the west, Srisailam in the northwest, Nallamalai in the east, Palnad in the northeast, and Kurnool in the central region. The Papaghni sub-basin (PSB) contains basic sills associated with the Paleoproterozoic carbonate-shale successions, whereas the Nallamalai sub-basin (NSB) consists of deformed Mesoproterozoic quartzite-phyllite successions and localized igneous intrusives. Subsequent to the deformation of the Cuddapah sediments, the Neoproterozoic Kurnool sub-basin (KSB) is developed over the deformed tracts of the Cuddapahs as a superposed basin in which the sediment accumulation pattern was controlled by ridge and depression type of topography **(Lakshminarayana et. al., 1999).** The rocks of Cuddapah Supergroup rests non-conformably over Peninsular Gneissic Complex. Shale/quartzite of Bairankonda Formation, and shale/phyllite, dolomite/ limestone and quartzite of overlying Cumbum Formation represent them. These rocks form the southern part of Cuddapah basin. The Bairankonda Formation consists mainly of fine to medium grained and thickly bedded quartzite. Intercalation of shale within the quartzite are seen at and near the western margin of the Cuddapah basin, notably east of Talakonda R.F and north of Tirupathi.

The Cumbum Formation consists mainly of shale, phyllite and quartzite with thin impersistent bands and lenses of

dolomite/limestone.

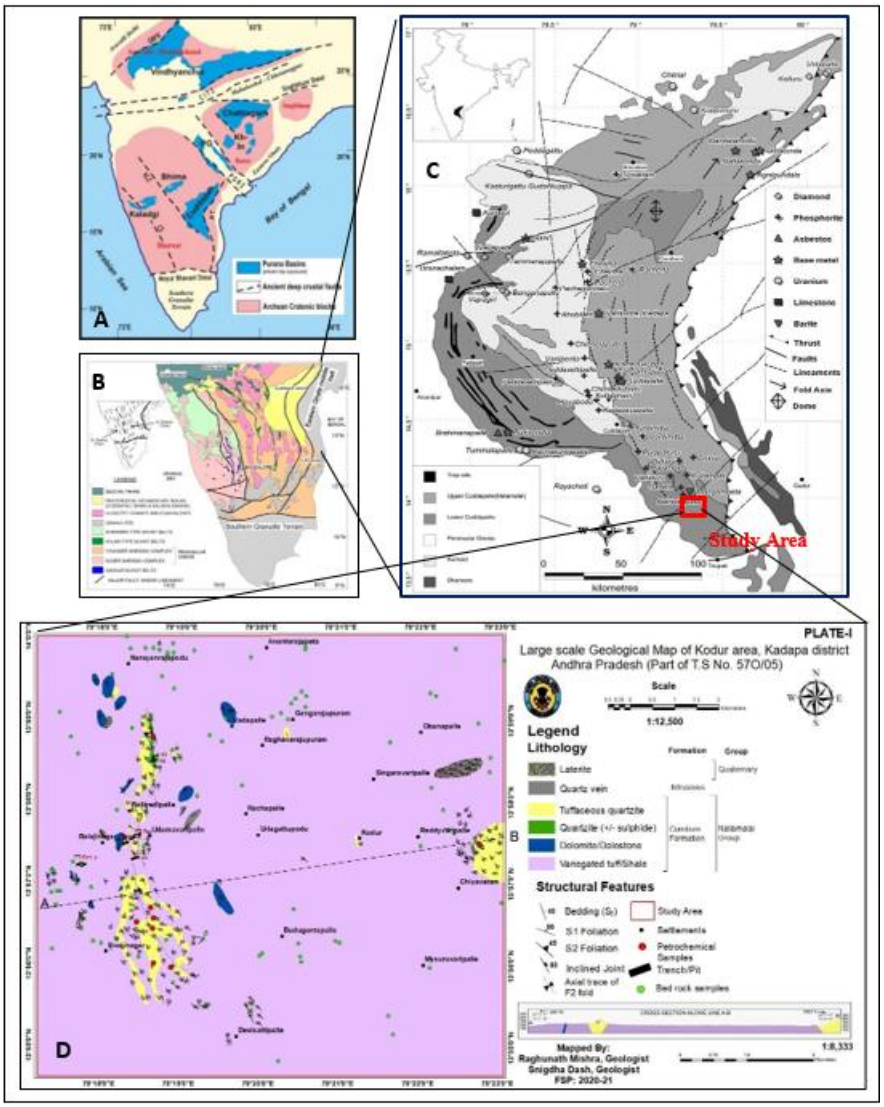


**Figure 1:** (A) Generalized tectonic map of India. (B) Geological map of the Dharwar craton, southern India showing Proterozoic Cuddapah basin (modified after Vasundhara Project, Geological Survey of India, 1994). CSZ: Chitradurga shear zone, CGL: Closepet Granite. (C) Geological map of Kadapa Basin (modified after Meijerink et al. 1984 and Nagaraja Rao et al. 1987) showing the locations of metallic and non-metallic resources. (D) Large scale geological map of Kodur area, Kadapa District, Andhra Pradesh, parts of Toposheet no. 57O/05 (after Mishra et al., 2021)

## 2. Study Area Geology and Stratigraphy

The study area is bounded by latitude 13°54'36.5" to 14°00'00"N and longitude 79°17'14.7" to 79°23'4.38" E of toposheet number 57O/05, which comes under Kadapa district of Andhra Pradesh (Fig.1). The rock types exposed in the area include variegated shale/tuff/slate/phyllite, dolomite, quartzite with sulphides, tuffaceous quartzite, quartz vein and laterite **(Mishra et al., 2021; Rao et al., 1976).** The Cumbum Formation comes under Nallamalai Group of Cuddapah Supergroup belonging to Mesoproterozoic age. The stratigraphy of the study area is given in table-1. During the course of mapping two phases of deformation were perceptible and has been noted. The two stages of deformation are omnipresent in the mapped area. The rocks of the area have a general NNW-SSE strike with gentle to moderate dips varying from 10°-45° towards ENE. Variations in strike and reversal of dip due to folding and swerving is common. The rocks are folded into a series of gently plunging anticlines and synclines with the fold axes trending NNW-SSE and plunging gently (10°-15°) generally towards NNW. The folds are open and symmetrical in nature. A synclinal folding along NNW-SSE axis is represented by gently and open warping's near Ballireddypalli area (Fig. 1).

Generally, the Cuddapah Supergroup is divided into Papaghni, Chitravati, Nallamalai and Kurnool Group from bottom to top, composed dominantly of argillaceous and arenaceous sediments with subordinate calcareous sediments **(Rao et al., 1987).** The study area comprises of rocks belonging to Nallamalai Group of Cumbum Formation (Table.1). The lithotypes comprises of variegated shale/tuff/slate/phyllite (argillaceous), dolomite/dolostone (calcareous) followed by quartzites (+/- sulphides) and tuffaceous quartzite (arenaceous). Here, we have considered the argillaceus (shale) and arenaceous (quartzites) lithounit for our study.

**Table 1:** Lithostratigraphy of Cuddapah Supergroup in study area

| Lithology | Formation | Group | Supergroup | Age |
|---|---|---|---|---|
| Top soil/Laterite | Quaternary | | | |
| Quartz vein | Intrusives | | | |
| Tuffaceous Quartzite | Cumbum formation | Nallamallai Group | Cuddapah Supergroup | Mesoproterozoic |
| Quartzite ± sulphides | | | | |
| Dolomite/ Dolostone | | | | |
| Variegated Shale/ tuff/ Slate/ Phyllite | | | | |

**Description of the rock types and petrographic studies**

The Nallamallai Group towards the southern part of the Cuddapah basin, denoted as Cumbum formation were characterised by typical quartzite, shale, dolomite intercalations. During the course of mapping intercalated sequences of quartzite/crystal tuff, ferrugenised quartzite, sulphide bearing quartzite, variegated shale/ tuffaceous shale, dolomitic limestone units has been marked in the study area.

The shale lithounit comprises of variegated shale (Fig. 2a) which is fine-grained and often bedded, with a predominantly weathered appearance. It frequently contains interbedded tuffaceous material and quartz grains of various sizes in a cryptocrystalline matrix. Its fissility plane causes it to break into flat sheets. Greyish-Yellowish shale is fine grained feeble bedded rock with fine laminae of olive green inter bands. It is characterized by the presence of a few centimetres' thick cherty nature quartzite/quartz crystal tuff (Fig. 2b). It is composed of subangular quartz, sericite, clay, pyrite, zircon and tourmaline. Finely laminated, reddish-buff flesh red tuff (Fig. 2c). exhibiting varying laminae thickness from millimeters to 5 centimeters. consisting of quartzo-feldspathic material, with patches of iron oxide resulting from pyrite leaching is noted in study area. Olive green shale extremely fine-grained with laminae typically 2 cm to 4 cm thick (Fig. 2d). Bluish grey to grey, greyish black, brownish at places, medium to fine grained, hard, compact and massive quartzite with sub-concoidal to concoidal fracture composed mainly of quartz with accessory amounts of calcareous (Fig. 2e) is observed. At places, it exbibits colour banding and depicts thinly bedded nature. It occurs as one centimetre to a few tens of cm's thick bands alternating with tuff beds and as massive unit ranging in thickness from a few metres to 20 mts (Fig. 2f).

Under thin section variegated shale with angular quartz grains appear to be in a dusty clayey matrix and with some feldspar. A very pervious foliation ($S_1$) is observed to be crosscutting the original bedding $S_0$ (Fig.3a). Flesh red to buff coloured shale have sericite, biotite noticed in abundant, followed by quartz (stretched augens), plagioclase, chlorite, zircon and tourmaline (Fig. 3b). The abundancy of sericite indicates that the tuffaceous rocks are subjected to intense weathering. The olive green tuff have needle shaped acicular grains of sericite admixed in the matrix. Plagioclase felspar, tourmaline, pyrite and zircon are the associated minerals. Near Urlagattupodu, Udumavaripalli where the tuffaceous rocks are in contact with dolostone, carbonate veins are observed cross cutting the olive buff coloured shale (Fig. 3c). In the tuffaceous quartzite ± sulphide, the constituent minerals identified are sub-angular to angular quartz, K-feldspar, plagioclase, sericite, carbonate, pyrite and tourmaline, of which quartz is the principal mineral constituent while others constitute accessories. It is fine grained (10µm to 80µm) with broken and embayed grains of quartz (Fig. 3d). Tuffaceous quartzite shows interlayering with variegated tuff which are often folded in micro scale (Fig. 3e). Some of the quartz grains are stretched and at places sheared porphyroblastic texture noticed (Fig. 3f).

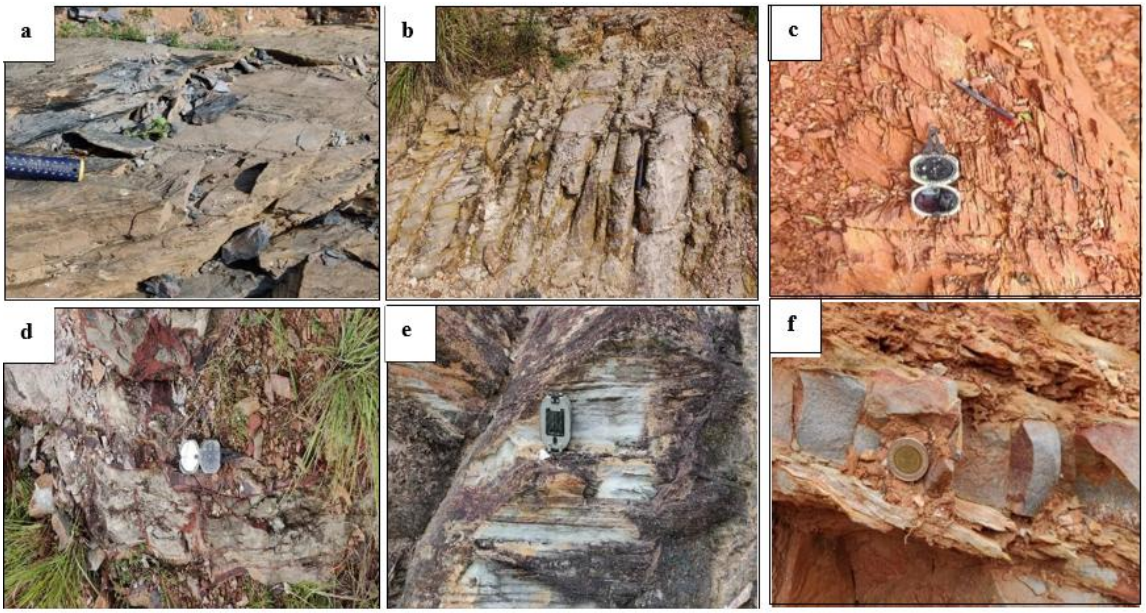


**Figure 2 (**A) Fine grained variegated shale, near Gundala Eru river bank, Kodur (B) grey-yellowish tuff, with pale yellow interbands, Tunakonda RF (C) foliated flesh red to buff coloured tuff, Udumavaripalli (D) Olive green tuff with buff red

interbands, Tunakonda RF (E) Tuffaceous quartz crystal tuff/quartzite, east of Balireddypalli (F) Thinly bedded tuffaceous quartz crystal tuff/quartzite, Balireddypalli.

Near Urlagattupodu, Udumavaripalli where the tuffaceous rocks are in contact with dolostone, carbonate veins are observed cross cutting the olive buff coloured shale (Fig. 3c). In the tuffaceous quartzite ± sulphide, the constituent minerals identified are sub-angular to angular quartz, K-feldspar, plagioclase, sericite, carbonate, pyrite and tourmaline, of which quartz is the principal mineral constituent while others constitute accessories. It is fine grained (10µm to 80µm) with broken and embayed grains of quartz (Fig. 3d). Tuffaceous quartzite shows interlayering with variegated tuff which are often folded in micro scale (Fig. 3e). Some of the quartz grains are stretched and at places sheared porphyroblastic texture noticed (Fig. 3f).

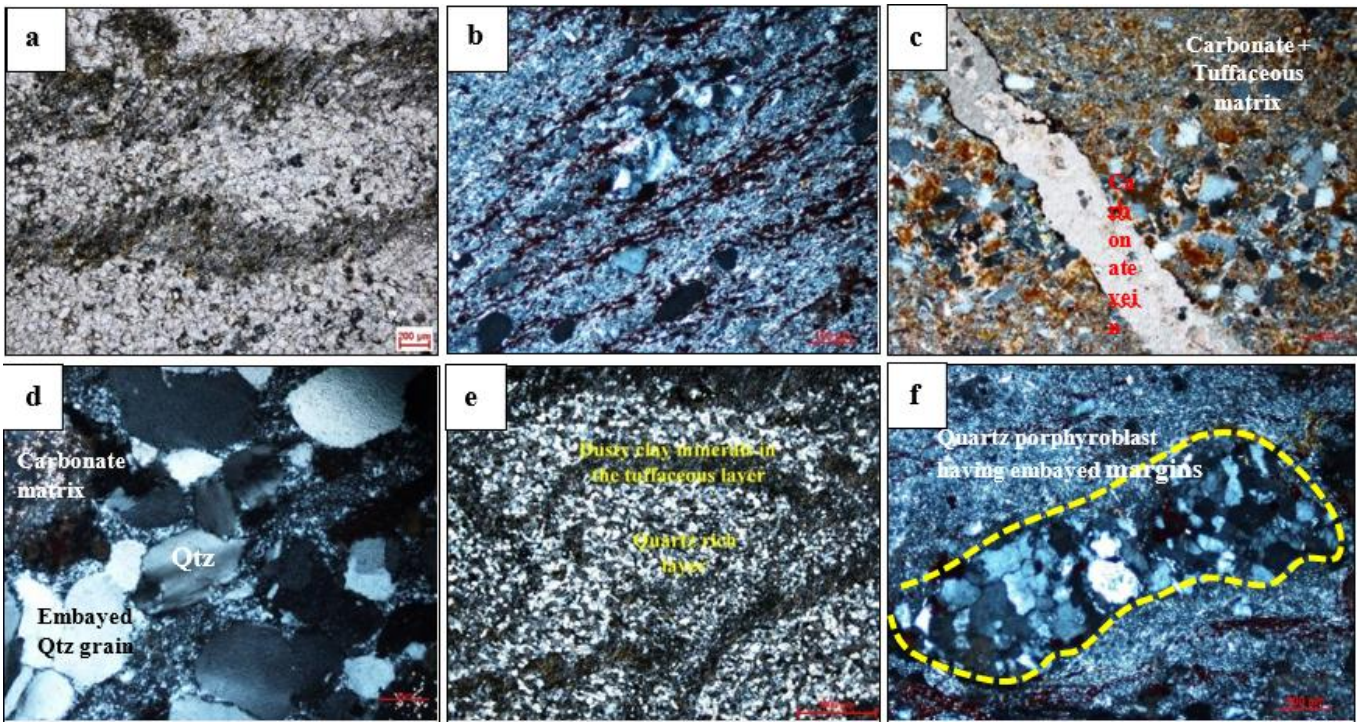


**Figure 3:** (A) Photomicrograph of variegated shale/tuff with distinct alignment of platy minerals (S1) , Udumavaripalle (B) buff tuff with stretched quartz augens, Buduguntapalle (C) olive green tuff with carbonate bands,east of Udumavaripalle (D) quartz crystal tuff within carbonate matrix in XPL, Buduguntapalle. (E) variegated tuff with arenaceous interbands Balireddypalli. (F) a quartz porphyroblast within matrix of variegated tuff, Buduguntapalle.

## 3. Materials and Methods

Representative fresh bed rock samples were collected from shale and quartzite lithounit for whole rock analysis. For whole rock analysis analytical results of 08 samples, 4 nos. samples from shaly horizon consisting of shaly quartzite and variegated shale, 4 nos. samples from quartzite unit comprising quartzite, banded ferruginized quartzite, ferrugenized quartzite and sulphide bearing quartzite are analysed. In addition, a total of 30 nos. of bed rock samples collected from carbonaceous shale lithounit exposed in the area were selected for major oxides and trace element analysis. The various types of lithounit were cut in to smaller sizes by diamond wheel saw (Carl-Zeiss) and thin section were prepared for petrographic studies. Detailed ore microscopic studies have been conducted to study the mineralogy, texture and microstructural aspects.

Fresh rock samples were crushed and pulverized to -200-micron size for chemical analysis. Whole rock analysis for major oxides by XRF and for trace elements, REE by ICP-MS was carried out in the Chemical Division, GSI, SR Hyderabad. Utmost care was taken during collection of samples and altered portions were strictly avoided. Major, minor and trace elements content of the rock were analysed using M/S Panalytical; MAGIX, 2.4 kW sequential X-Ray Fluorescence (XRF) Spectrometer using pressed pellet method which is having a detection limit of 0.1% for major and minor elements and 1.00 ppm for trace elements. Precision of the instrument is ± 10%. Rare earth elements were analysed using a Perkin Elmer Sciex ELAN 6100 inductively coupled plasma mass spectrometer (ICP-MS) with fusion method having quantification limits from 0.10 to 1 ppm and precision of ± 10%. All the data sets were processed using GCD-Kit software. Major elements data for representative samples as well as averages of PAAS (Post-Archaean Australian shale) and UCC (Upper continental crust) from the shale and quartzite lithounits are given in Table.2. The trace element contents of 08 selected samples from the study area as well as averages of PAAS (Post-Archaean Australian shale) and UCC (Upper continental crust) belonging to shale and quartzite lithounits are given in Table 4.

Mineral phase chemistry analysis was carried out on CAMECA SX100 electron microprobe at EPMA laboratory, Petrology Division, Geological Survey of India, Southern Region, Hyderabad. The analysis was performed under

conditions of 15 kV accelerating voltage and 15nA beam current keeping the beam diameter at 1 micron.

## 4. Results and Discussion

**Whole Rock Geochemistry Major Oxides**

Major elements data for representative samples as well as averages of PAAS (Post-Archaean Australian shale) and UCC (Upper continental crust) from the shale and quartzite lithounits are given in Table 2. Among these PCS-02, PCS-03, PCS-05 and PCS-07 belongs to shale lithounit and the remaining ones belongs to quartzite lithounit. Each rock type comprises a distinct geo-chemical group as shown for instance by the distribution of SiO2 and Fe2O3.

The quartzites of Cumbum formation has higher SiO2 contents (88.05%) than the variegated shales and shaly quartzites of Cumbum (Table 2). The studied metasedimentary rocks generally have $SiO_2$ (64.22%–67.26%) wt.%, $Al_2O_3$ (20.3%–21.58%) wt.%, TiO2 (0.67%–0.84%) wt.% and $K_2O$ (5.19%–5.98%) wt.% contents similar to that of PAAS (Fig 5.47). However, $Fe_2O_3$ (2.48%-3.57%) wt.%, MgO (0.1) wt.%, $Na_2O$ (0.11%–0.15) wt.% and CaO (0.10%–0.16%) wt.% contents are depleted compared to that of PAAS (Fig. 4). The $P_2O_5$ content of the rocks varies from 0.02-0.03%, with an average of 0.03% (Fig. 4). They have low $SiO_2/Al_2O_3$ values (2.97 to 3.31) indicative of their low maturity. SiO2 correlates negatively with $Al_2O_3$ (r = −0.99), $TiO_2$ (r = −0.98), $K_2O$ (r = −0.83) $Na_2O$ (r= −0.55) and $P_2O_5$ (r= −0.17)

(Table 3 co-relation matrix table). MnO (r=0.46), MgO (r= 0.56) and CaO (r= 0.46) show moderately +ve corelation with $SiO_2$. However, $Al_2O_3$ shows strong +ve corelation with $K_2O$ (r=0.85) and $TiO_2$ (r=0.98), and moderately +ve corelation with $Na_2O$ (r=0.56) except for weak negative correlation with $Fe_2O_3$ (−0.19), MnO (r=−0.41), MgO (r= −0.57) and CaO (r= −0.43) (Table. 3).

The shale and quartzite samples were normalized to PAAS (Taylor, S.R., McLennan, S.M., 1985) and UCC (Rudnick R. L., Gao S., 2003) as depicted in Fig.4. In comparison with PAAS, the average concentrations of $SiO_2$, $TiO_2$, $Al_2O_3$ and $K_2O$ are 1.04, 0.76, 1.10,1.51 respectively, which are generally comparable with PAAS. Conversely, the average concentration of Fe2O3, MnO, MgO, CaO, $Na_2O$ and $P_2O_5$ relative to PAAS is low, averaging 0.42, 0.09, 0.04, 0.11 and 0.15. Relative to UCC, the average concentrations of SiO2, Fe2O3 and K2O in the quartzites are 1.32, 0.72, and 0.58, respectively, which are generally comparable with the UCC. On the other hand, the average concentration of $TiO_2$, $Al_2O_3$, MnO, MgO, CaO, $Na_2O$ and $P_2O_5$ relative to UCC are 0.13, 0.25, 0.12, 0.05, 0.04, 0.03 and 0.20, respectively, which are generally low as compared to UCC. The depletion of $Na_2O$ (< 1%) in the quartzites can be attributed to a relatively smaller amount of Na-rich plagioclase in them. $K_2O$ and $Na_2O$ contents and their ratios (K2O/Na2O > 1) revealed that K-feldspar dominates over plagioclase (albite) feldspar. $K_2O$ enrichment relates to the presence of illite as common clay mineral in the shales and quartzites. Relative to UCC, the shales are low in MnO, MgO, CaO, Na2O and $P_2O_5$ and high in $SiO_2$, $TiO_2$, $Fe_2O_3$, $Al_2O_3$ and $K_2O$. Al and Ti are easily absorbed on clays and concentrate in the finer, more weathered materials **(Das, B.K., AL-Mikhlafi, A.S., Kaur, P., 2006).**

**Table 2:** Major element contents with statistical data of PCS samples collected from different lithounits of the study area.

| Sample | PCS-01 Quartzite | PCS-02 Shale | PCS-03 Shale | PCS-04 Quartzite | PCS-05 Shale | PCS-06 Quartzite | PCS-07 Shale | PCS-08 Quartzite | Avg. | PAAS | UCC |
|---|---|---|---|---|---|---|---|---|---|---|---|
| SiO2 | 84.39 | 65.14 | 65.20 | 85.29 | 67.26 | 90.92 | 64.22 | 91.61 | 76.75 | 62.80 | 66.6 |
| Al2O3 | 6.82 | 20.62 | 21.07 | 3.87 | 20.30 | 3.18 | 21.59 | 1.84 | 12.41 | 18.90 | 15.4 |
| Fe2O3 | 0.52 | 3.36 | 2.81 | 8.08 | 2.48 | 3.58 | 3.57 | 2.47 | 3.36 | 7.23 | 5.04 |
| MnO | 0.01 | 0.01 | 0.01 | 0.01 | 0.01 | 0.02 | 0.01 | 0.01 | 0.01 | 0.11 | 0.1 |
| MgO | 0.10 | 0.10 | 0.10 | 0.14 | 0.10 | 0.10 | 0.10 | 0.25 | 0.12 | 2.20 | 2.48 |
| CaO | 0.10 | 0.10 | 0.16 | 0.10 | 0.10 | 0.13 | 0.10 | 0.35 | 0.14 | 1.30 | 3.59 |
| Na2O | 0.16 | 0.15 | 0.11 | 0.10 | 0.14 | 0.10 | 0.15 | 0.10 | 0.13 | 1.20 | 3.27 |
| K2O | 5.54 | 5.19 | 5.98 | 0.10 | 5.33 | 0.10 | 5.87 | 0.77 | 3.61 | 3.70 | 2.8 |
| TiO2 | 0.13 | 0.84 | 0.67 | 0.11 | 0.74 | 0.02 | 0.80 | 0.08 | 0.42 | 1.00 | 0.64 |
| P2O5 | 0.03 | 0.02 | 0.03 | 0.03 | 0.02 | 0.02 | 0.03 | 0.02 | 0.03 | 0.16 | 0.12 |
| L.O.I | 1.52 | 4.20 | 3.85 | 2.35 | 3.60 | 1.72 | 3.59 | 2.10 | 2.87 | -- | -- |

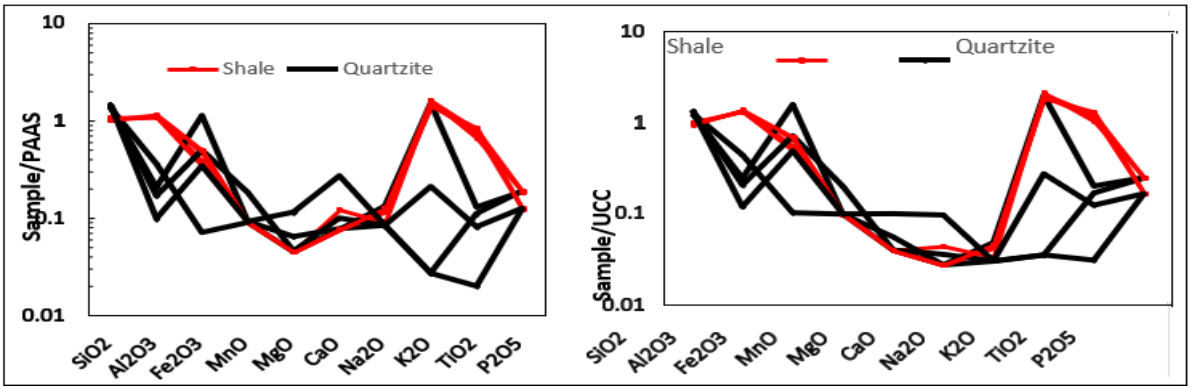


**Figure 4:** Post-Archaean Australian Shale (PAAS)-normalised and UCC normalised major element for the studied samples from shale and quartzite litho-unit {after Rudnick R. L., Gao S. (2003) and Taylor, S.R., McLennan, S.M. (1985)}

**Table 3:** Correlation matrix of major oxides for of PCS samples collected from shale and quartzite lithounit of the study area

| | SiO2 | Al2O3 | Fe2O3 | MnO | MgO | CaO | Na2O | K2O | TiO2 | P2O5 |
|---|---|---|---|---|---|---|---|---|---|---|
| SiO2 | 1.00 | | | | | | | | | |
| Al2O3 | -0.99 | 1.00 | | | | | | | | |
| Fe2O3 | 0.11 | -0.19 | 1.00 | | | | | | | |
| MnO | 0.46 | -0.41 | 0.04 | 1.00 | | | | | | |
| MgO | 0.56 | -0.57 | 0.07 | -0.18 | 1.00 | | | | | |
| CaO | 0.46 | -0.43 | -0.19 | -0.06 | 0.92 | 1.00 | | | | |
| Na2O | -0.55 | 0.56 | -0.51 | -0.41 | -0.52 | -0.52 | 1.00 | | | |
| K2O | -0.83 | 0.85 | -0.55 | -0.52 | -0.56 | -0.40 | 0.80 | 1.00 | | |
| TiO2 | -0.98 | 0.98 | -0.14 | -0.44 | -0.47 | -0.37 | 0.55 | 0.79 | 1.00 | |
| P2O5 | -0.17 | 0.11 | 0.19 | -0.38 | -0.28 | -0.34 | 0.15 | 0.30 | 0.01 | 1.00 |

All the four samples of quartzite show high concentration of $SiO_2$, ranging from 84.39% to 91.61%. The $Al_2O_3$, CaO and $Fe_2O_3$ contents are moderately high, ranging from 1.84 to 6.82%, 0.1 to 0.35% and 0.52 to 8.08%, respectively. The concentrations of $TiO_2$, MnO, MgO, $Na_2O$, $K_2O$ and $P_2O_5$ are generally low, ranging from 0.02 to 0.13%, 0.01 to 0.02%, 0.1 to 0.25%, 0.1 to 0.16%, 0.1 to 5.54% and 0.02 to 0.03%, respectively (Fig.5). The quartzites are higher in SiO2 content more than the shales. On the other hand, shales are higher in $Fe_2O_3$, $K_2O$ and $TiO_2$ contents more than the quartzites (Table. 2), which reflect their association with clay-sized phases (Madhavaraju, J., Lee, Y.I., 2010). The abundance of Al2O3 was used as a normalization factor to make comparisons among the different lithologies because of their immobile nature during weathering, diagenesis and metamorphism **(Bauluz, B., Mayayo, M.J., Fernandez-**Nieto, C., Gonzalez-Lopez, J. M, Major; 2000). Oxides of the studied shales and quartzites were plotted against $Al_2O_3$ as depicted in (Fig.6). In addition, average UCC (Upper Continental Crust) and PAAS (Post-Archaean Australian Shale) values were extracted from (Taylor, S.R., McLennan, S.M., 1985) and (Rudnick R. L., Gao S., 2003), respectively and included in the plots for comparison purposes. In the shale samples, major elements like $TiO_2$, $Fe_2O_3$ and $K_2O$ shows positive correlation with Al2O3, whereas MnO, CaO, $Na_2O$ and $P_2O_5$ shows no particular trend (Fig. 6). Similarly, in the quarztite samples, $TiO_2$ and $P_2O_5$ shows positive correlation with $Al_2O_3$, while MnO, CaO and $Na_2O$ shows no particular trend and with increase of SiO2, Al2O3 decreases (Fig. 6).

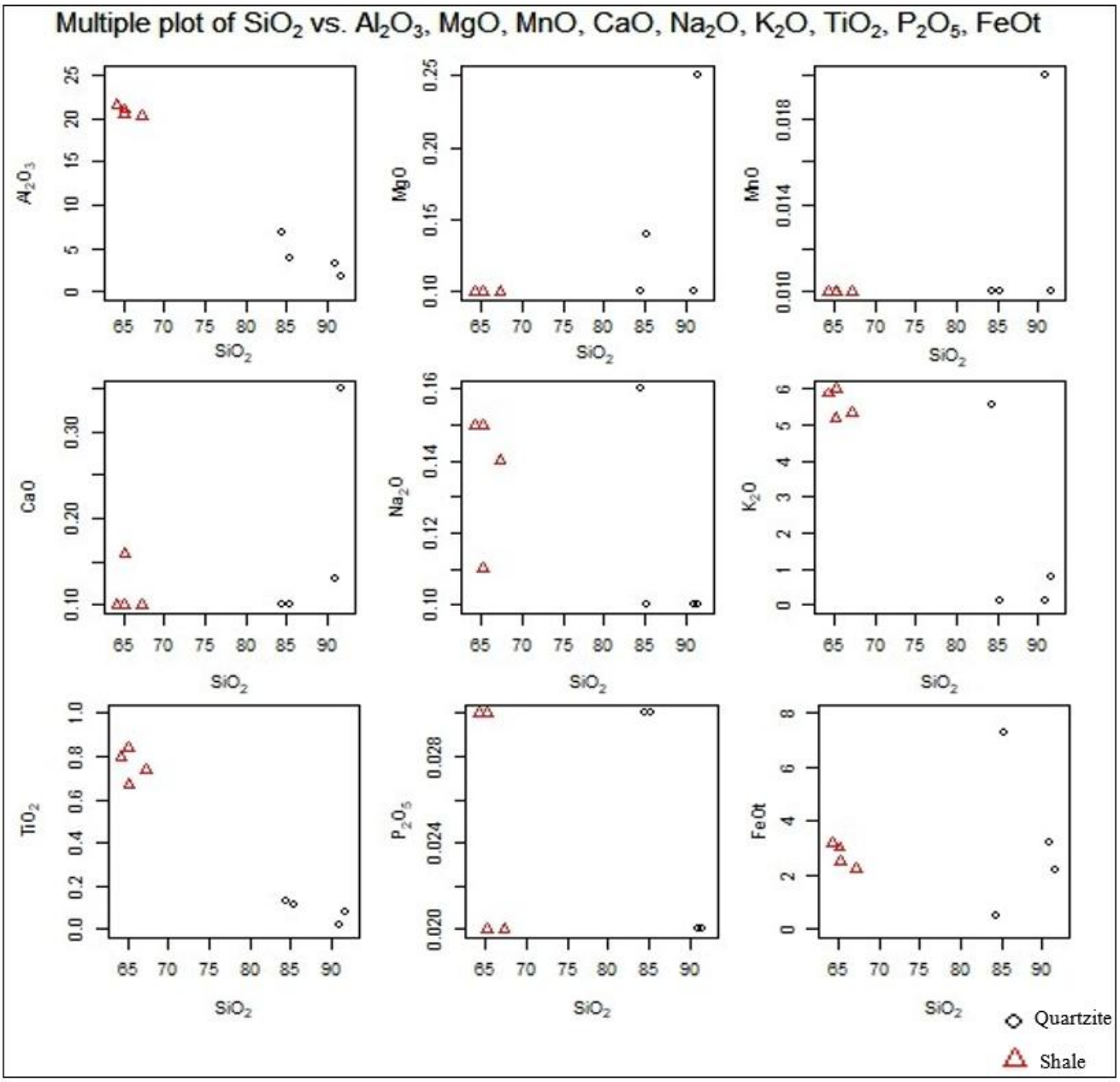


**Figure 5:** Harker plot of $SiO_2$ vs major oxides of shale and quartzite litho-unit of the study area.

Several workers have used major element whole rock geochemistry to classify siliciclastic sedimentary rocks (e.g. Blatt, Middleton, & Murray, 1980; Crook, 1974; Herron, 1988; Pettijohn, Potter, & Siever, 1972). By their $Fe_2O_3/K_2O$ versus $SiO_2/Al_2O_3$ the studied samples classify as shales (Fig. 7). Out of four quartzite samples one sample falls in the sub-arkose field and the rest three falls in Fe-sand field.

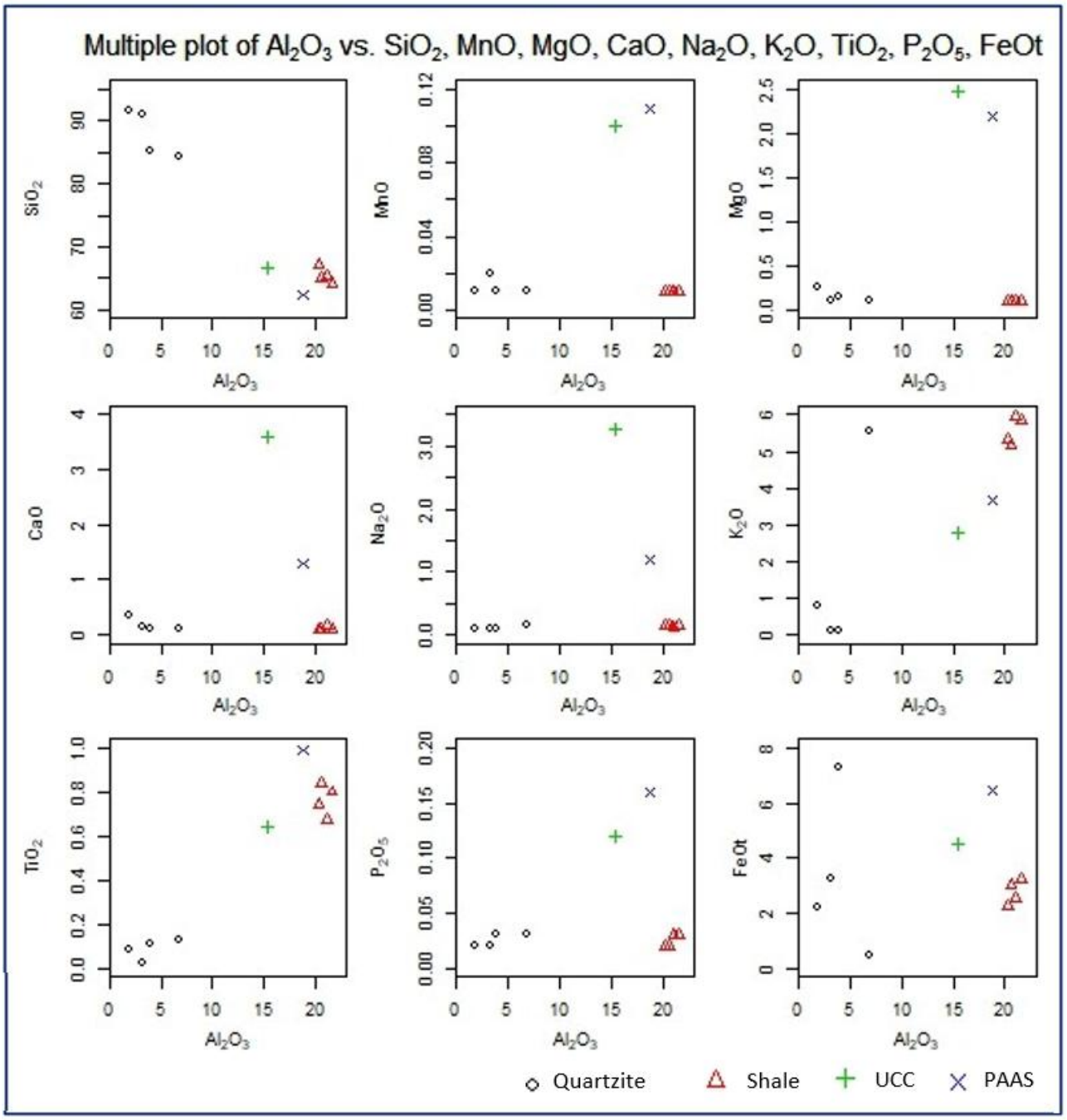


**Figure 6:** Major elements versus Al2O3 graph showing the distribution of shale and quartzite samples from the Study area. Average data of UCC and PAAS from Rudnick R. L., Gao S. (2003) and Taylor, S.R., McLennan, S.M. (1985), respectively are also plotted for comparison.

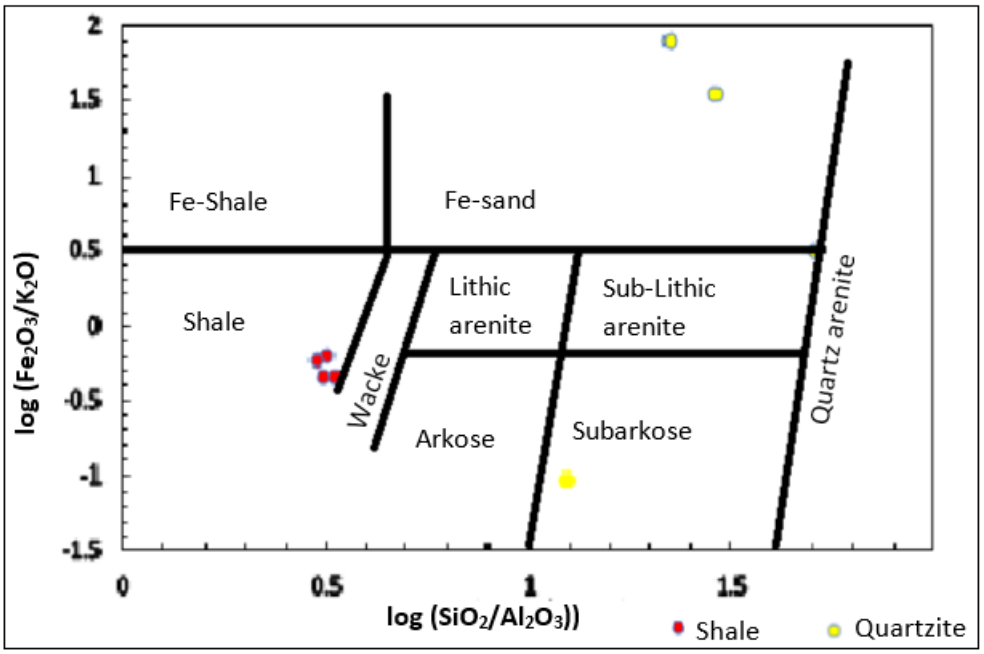


**Figure 7:** Classification of the studied metasedimentary rocks using log (Fe2O3/K2O) versus log (SiO2/Al2O3) (after Herron, 1988).

**Trace Elements:**

The trace element contents of eight selected samples from the study area as well as averages of PAAS (Post-Archaean Australian shale) and UCC (Upper continental crust) belonging to shale and quartzite lithounits are given in Table. 4 out of which PCS-02, PCS-03, PCS-05 and PCS-07 belongs to shale lithounit. The concentrations of the large ion lithosphere elements (LILE) Rb, Ba, Sr and Th range from 210.45 to 250.25 ppm, 344.14 to 592.27 ppm, 18.44 to 43.31 ppm and 19.47 to 26.01 ppm, respectively (Table. 4).

In comparison to PAAS, the studied shales exhibit slight to strong depletion in Sr, Co and Ni and enrichment in Ba, Rb, Cr and Nb. The shales are having a marked depletion in Sr (~ 18.44–43.31 ppm; Fig.8. These shales have a relatively low Ba enrichment and this Ba enrichment in sedimentary rocks can be considered as an indicator of detrital flux. Some trace elements such as Cr, Sc, Ni, and V are positively correlated (Table. 5) with Al2O3 (r = 0.58, r = 0.72, r = 0.74, r = 0.63, respectively), which suggest that these elements may be bound in clay minerals and concentrated during weathering **(*e.g.*, Fedo *et al.*, 1996)**. Rb/Sr ratios (5.24 to 13.57) are lower than that of PAAS (Rb/ Sr = 7.00; **Taylor & McLennan, 1985) (**Table 6).

The studied shales have high so-called transition metals Ni (2 to 7.37 ppm, average of 3.83 ppm), Co (1.34 to 8.59, average of 5.61 ppm), Cr (104.75 to 135.09 ppm, with an average of 118.20 ppm), V (96.92 to 139.12 ppm, with average of 120.06 ppm), and Sc (17.03 to 22.63 ppm, with an average of 19.39 ppm). Generally, the studied shales are enriched in these transition metals relative to PAAS except for Ni and Co (Fig. 8).

**Table 4:** Trace element contents with statistical data of PCS samples collected from different litho-units of the study area.

| Sample | PCS-1 | PCS-2 | PCS-3 | PCS-4 | PCS-5 | PCS-6 | PCS-7 | PCS-8 | Avg. | PAAS | UCC |
|---|---|---|---|---|---|---|---|---|---|---|---|
| Trace Elements (ppm) | Quartzite | Shale | Shale | Quartzite | Shale | Quartzite | Shale | Quartzite | | | |
| Ba | 1270.42 | 344.14 | 592.27 | 51.53 | 546.69 | 104.05 | 357.82 | 749.40 | 502.04 | 650 | 550 |
| Ga | 5.00 | 23.22 | 20.23 | 6.91 | 19.66 | 6.32 | 22.34 | 5.00 | 13.59 | 20.00 | 17 |
| Sc | 3.50 | 20.02 | 17.63 | 11.77 | 17.30 | 5.77 | 22.63 | 3.50 | 12.77 | 16.00 | 13.6 |
| V | 20.00 | 134.05 | 110.16 | 31.36 | 96.92 | 20.00 | 139.12 | 20.00 | 71.45 | 150.00 | 107 |
| Th | 6.64 | 24.31 | 19.47 | 4.00 | 26.01 | 4.00 | 21.28 | 4.00 | 13.71 | 14.60 | 10.7 |
| Pb | 19.43 | 17.48 | 4.57 | 5.79 | 8.09 | 6.82 | 18.04 | 13.25 | 11.68 | 20.00 | 17 |
| Ni | 2.00 | 3.95 | 2.00 | 2.00 | 2.00 | 2.00 | 7.37 | 2.00 | 2.92 | 55.00 | 44 |
| Co | 2.04 | 5.53 | 8.59 | 3.08 | 7.01 | 6.03 | 1.34 | 2.64 | 4.53 | 23.00 | 17 |
| Rb | 84.85 | 216.78 | 250.25 | 6.17 | 210.45 | 5.00 | 227.11 | 17.76 | 127.30 | 160.00 | 112 |
| Sr | 24.69 | 35.77 | 18.44 | 5.55 | 31.70 | 5.18 | 43.31 | 24.90 | 23.69 | 200.00 | 350 |
| Y | 10.92 | 25.12 | 23.16 | 7.96 | 20.88 | 5.50 | 23.89 | 6.52 | 15.49 | 27.00 | 22 |
| Zr | 480.41 | 232.29 | 263.03 | 114.42 | 261.21 | 34.94 | 181.81 | 315.96 | 235.51 | 210.00 | 190 |
| Nb | 5.00 | 13.24 | 11.55 | 5.00 | 12.44 | 5.00 | 12.01 | 5.00 | 8.66 | 1.90 | 25 |
| Cr | 15.00 | 127.21 | 105.76 | 46.76 | 104.75 | 75.78 | 135.09 | 15.00 | 78.17 | 110.00 | 83 |
| Cu | 6.03 | 5.25 | 2.27 | 4.43 | 0.88 | 5.49 | 1.34 | 29.50 | 6.90 | 50.00 | 25 |
| Zn | 10.00 | 16.26 | 22.20 | 10.00 | 11.32 | 10.00 | 10.00 | 33.21 | 15.37 | 85.00 | 71 |
| U | 4.55 | 4.43 | 3.48 | 3.06 | 4.51 | 4.80 | 5.31 | 3.68 | 4.23 | 14.60 | 2.8 |
| Hf | 16.27 | 6.11 | 6.70 | 5.79 | 6.51 | 3.48 | 4.76 | 10.67 | 7.54 | 5.00 | 5.8 |

The concentrations of the high field strength elements (HFSE), Zr, Hf, Y, Nb, Th and La range from 181.81 to 263.03 ppm, 4.76 to 6.70 ppm, 20.88 to 25.12 ppm, 11.55 to 13.24 ppm, 19.47 to 26.01 ppm and 15.16 to 33.67 ppm, respectively. Relative to PAAS the studied shales exhibit enrichment in the HFSE (Fig. 8). The average Zr/Hf (Table. 6) value of 38.89 is suggestive of zircon control (Zr ≈ 40). Th/U values (5.49 to 5.78) are consistently higher (Table. 6) than that of the continental upper crust (Th/U ≈ 3.8; McLennan, Hemming, McDaniel, & Hanson, 1993).

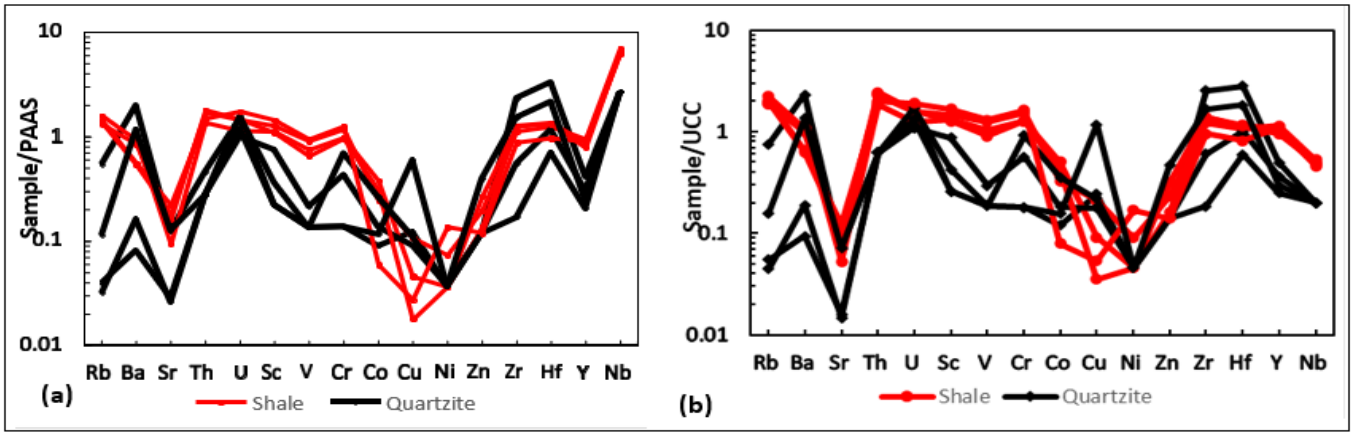


**Figure 8:** Trace element concentrations of the study are samples normalised to the composition of average PAAS and UCC (Taylor and McLennan (1985).

The trace element compositions are quite variable but still comparable with the average compositions documented **by (Gromet, L.P., Dymek, R.F., Haskin, L.A., Korotev, R.L., 1984 and Levinson, A.A., 1974)**. In the quartzites, the contents of large ion lithophile elements (LILE) like Rb, Ba, Sr and Th vary from 5 to 84.85 ppm, 51.53 to 1270.42 ppm, 5.18 to 24.90 ppm and 4 to 6.64 ppm, respectively. In comparison to UCC, the studied quartzites exhibit slight to strong depletion in Rb, Ba and Sr and enrichment in Th and U among the LILE (Fig. 8). The content of high field strength elements (HFSE) like Zr, Y and Nb range from 34.94 to 480.41 ppm, 5.5 to 10.92 ppm and 5 ppm, respectively. Relative to UCC the studied quartzites exhibit enrichment in the HFSE except for Y and Nb (Fig.8). Similarly, transition trace elements (TTE) like Sc, V, Cr, Ni and Zn range from 3.5 to 11.77 ppm, 20 to 31.36 ppm, 15 to 75.78 ppm, 2 ppm and 10 to 33.21 ppm, respectively. Generally, the studied quartzites show slight depletion to flat pattern in the transition metals relative to UCC except for Ni showing a strong depletion pattern. The concentrations of Zr, Hf and Y in the quartzites are comparable with the UCC contents (Fig. 8) whereas Nb is depleted.

Based on the LILE average values, except for Sr and Ba, almost all the shale samples exhibit similar LILE abundances relative to UCC and PAAS (Fig. 8). In contrast, the quartzites exhibit similar Th and U contents relative to UCC and PAAS but are depleted in Rb, and Sr (Fig. 8). Th has very strong positive correlations with Nb in the shales and quartzites. This implies that it may have been controlled by clays and/or other phases associated with clay minerals. Rb and Ba are positively correlated in the quartzite and shales, perhaps indicating a similar geochemical behaviour. These correlations indicate that their distributions are mainly controlled by illites and other minor clays. The average contents of Zr in the shales are lower than those in the quartzites, which perhaps indicate that the mineral zircon tend to be preferentially concentrated in quartzite.

**Table 5:** Correlation matrix for of PCS samples for trace elements collected from the shale lithounit of the study area

| | *Al2O3* | *Ba* | *Ga* | *Sc* | *V* | *Th* | *Pb* | *Ni* | *Co* | *Rb* | *Sr* | *Y* | *Zr* | *Nb* | *Cr* | *Cu* | *Zn* |
|---|---|---|---|---|---|---|---|---|---|---|---|---|---|---|---|---|---|
| Al2O3 | 1.00 | | | | | | | | | | | | | | | | |
| Ba | -0.31 | 1.00 | | | | | | | | | | | | | | | |
| Ga | 0.34 | -0.94 | 1.00 | | | | | | | | | | | | | | |
| Sc | 0.72 | -0.86 | 0.79 | 1.00 | | | | | | | | | | | | | |
| V | 0.64 | -0.90 | 0.94 | 0.92 | 1.00 | | | | | | | | | | | | |
| Th | -0.80 | -0.16 | -0.03 | -0.22 | -0.28 | 1.00 | | | | | | | | | | | |
| Pb | 0.33 | -0.99 | 0.91 | 0.88 | 0.88 | 0.19 | 1.00 | | | | | | | | | | |
| Ni | 0.75 | -0.80 | 0.69 | 0.99 | 0.86 | -0.22 | 0.83 | 1.00 | | | | | | | | | |
| Co | -0.62 | 0.81 | -0.64 | -0.95 | -0.78 | 0.03 | -0.85 | -0.98 | 1.00 | | | | | | | | |
| Rb | 0.57 | 0.42 | -0.19 | -0.10 | 0.01 | -0.95 | -0.46 | -0.10 | 0.28 | 1.00 | | | | | | | |
| Sr | 0.26 | -0.86 | 0.64 | 0.82 | 0.66 | 0.36 | 0.90 | 0.83 | -0.92 | -0.63 | 1.00 | | | | | | |
| Y | 0.44 | -0.73 | 0.91 | 0.63 | 0.88 | -0.35 | 0.67 | 0.52 | -0.39 | 0.19 | 0.29 | 1.00 | | | | | |
| Zr | -0.74 | 0.81 | -0.69 | -0.99 | -0.85 | 0.20 | -0.84 | -1.00 | 0.98 | 0.12 | -0.84 | -0.51 | 1.00 | | | | |
| Nb | -0.56 | -0.60 | 0.57 | 0.13 | 0.27 | 0.76 | 0.58 | 0.04 | -0.13 | -0.78 | 0.46 | 0.34 | -0.05 | 1.00 | | | |
| Cr | 0.59 | -0.95 | 0.90 | 0.97 | 0.96 | -0.10 | 0.96 | 0.93 | -0.90 | -0.20 | 0.83 | 0.74 | -0.93 | 0.33 | 1.00 | | |
| Cu | -0.19 | -0.49 | 0.70 | 0.12 | 0.48 | 0.08 | 0.40 | -0.03 | 0.10 | -0.07 | 0.02 | 0.79 | 0.02 | 0.68 | 0.33 | 1.00 | |
| Zn | -0.04 | 0.47 | -0.16 | -0.50 | -0.19 | -0.54 | -0.56 | -0.57 | 0.73 | 0.74 | -0.86 | 0.24 | 0.58 | -0.27 | -0.45 | 0.42 | 1.00 |

**Table 6:** Rb/Sr, Zr/Hf and Th/U ratios for the studied shale samples from the study area

| Sample | | Rb | Sr | Rb/Sr | Zr | Hf | Zr/Hf | Th | U | Th/U |
|---|---|---|---|---|---|---|---|---|---|---|
| PCS-02 | Shale | 216.78 | 35.77 | 6.06 | 232.29 | 6.11 | 38.02 | 24.31 | 4.43 | 5.49 |
| PCS-03 | | 250.25 | 18.44 | 13.57 | 263.03 | 6.70 | 39.24 | 19.47 | 3.48 | 5.59 |
| PCS-05 | | 210.45 | 31.70 | 6.64 | 261.21 | 6.51 | 40.10 | 26.01 | 4.51 | 5.76 |
| PCS-07 | | 227.11 | 43.31 | 5.24 | 181.81 | 4.76 | 38.23 | 21.28 | 3.68 | 5.79 |

**Rare earth elements**:

Behaviour of REE in upper crustal environment has a great importance in studying sediments, sedimentary rocks and continental crust because they are not easily fractionated during sedimentary processes and therefore provide an index to average provenance composition **(McLennan, 1989)**. The rare earth element (REE) data for the studied shales are somewhat variable with total REE (ΣREE) values of ranging from 89.80 to 148.22 ppm, averaging of 108.92 ppm, which is lower than that of PAAS value of 184.8 ppm **(Taylor & McLennan, 1985)**. The shales display REE patterns that are similar when normalised to PAAS with slightly depleted Light REE (LREE) (Fig. 9) and fairly flat Heavy REE (HREE). On a chondrite-normalised diagram (Fig. 9) the studied shales display slightly enriched LREE patterns (average $La_N/Sm_N$ = 5.27), small negative Eu (average Eu/Eu* = 0.69) and fairly flat HREE patterns (average $Gd_N/Yb_N$ = 0.13) except for Yb which are characteristic of sediments derived from upper continental crust **(Taylor & McLennan, 1985)**.

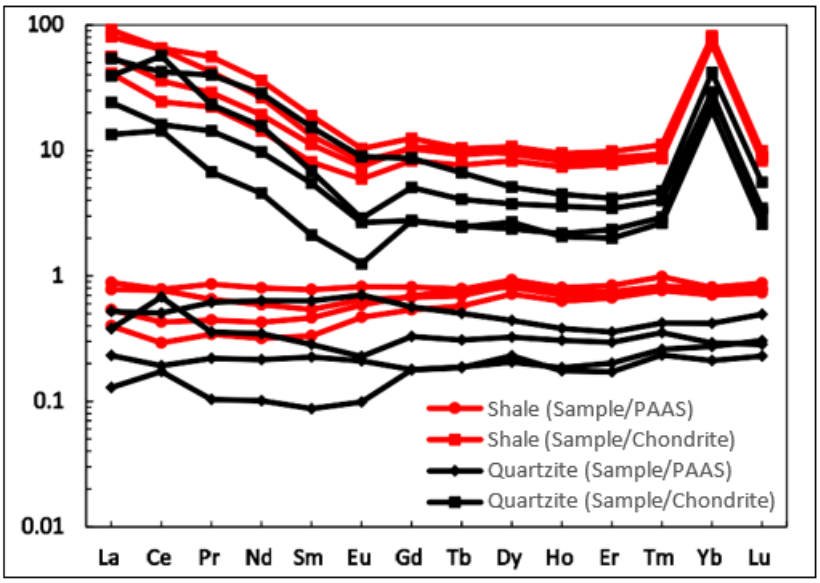


**Figure 9:** Rare earth element abundances of the studied shales and quartzites normalised to PAAS and chondrite. PAAS and chondrite values are from Taylor and McLennan (1985).

The results of REE analyses are listed in Table. 7 and are shown as chondrite-normalized patterns in Fig. 9. Total REE (ΣREE) abundances are variable throughout the succession (Table. 7). Quartzites have a wide range of total REE (ΣREE) contents of 26.91-98.15 ppm with an average 63.35 ppm (Table. 7) which is relatively less to that of the UCC (Taylor and McLennan, 1985). Compared to quartzites the shales have greater REE abundances (ΣREE contents of 65.38 - 148.22 ppm with an average about 108.93 ppm) suggesting that clays control the REE distributions (Hossain et al., 2010).

In general, chondrite-normalized REE patterns for the studied quartzites (Fig. 9) are characterized by high light REE/heavy REE (LREE/HREE) ratio (6.79 - 15.52, (Table. 7), flat HREE pattern except Yb and pronounced negative Eu anomaly. LREEs are fractionated, (La/Sm)n = 4.98 and the HREE patterns are almost flat, (Gd/Yb)n =0.15. This chondrite-normalized pattern is typical of sediments and sedimentary rocks enriched in light REE (LREE), flat heavy REE (HREE) and negative Eu anomaly (Borges et al., 2008). The europium anomaly of quartzites is always negative, ranging from 0.49 to 0.77 (average 0.62) which is quite typical to that of UCC (0.62) and PAAS (0.59).

**Table 7:** Rare earth element concentrations (ppm) of quartzites of study area

| Sample | PCS-01 | PCS-04 | PCS-06 | PCS-08 | Average | Chondrite | PAAS | UCC |
|---|---|---|---|---|---|---|---|---|
| | Quartzite | | | | | | | |
| La | 19.76 | 4.90 | 14.38 | 8.84 | 11.97 | 0.37 | 38.00 | 30.00 |
| Ce | 40.34 | 13.79 | 54.18 | 15.35 | 30.92 | 0.96 | 80.00 | 64.00 |
| Pr | 5.47 | 0.92 | 3.17 | 1.96 | 2.88 | 0.14 | 8.90 | 7.10 |
| Nd | 20.31 | 3.24 | 11.11 | 6.90 | 10.39 | 0.71 | 32.00 | 26.00 |
| Sm | 3.55 | 0.49 | 1.58 | 1.26 | 1.72 | 0.23 | 5.60 | 4.50 |
| Eu | 0.77 | 0.11 | 0.25 | 0.23 | 0.34 | 0.09 | 1.10 | 0.88 |
| Gd | 2.65 | 0.84 | 1.55 | 0.84 | 1.47 | 0.31 | 4.70 | 3.80 |

| | | | | | | | | |
|---|---|---|---|---|---|---|---|---|
| Tb | 0.39 | 0.14 | 0.24 | 0.14 | 0.23 | 0.06 | 0.77 | 0.64 |
| Dy | 1.94 | 1.02 | 1.43 | 0.90 | 1.32 | 0.38 | 4.40 | 3.50 |
| Ho | 0.38 | 0.17 | 0.31 | 0.19 | 0.26 | 0.09 | 1.00 | 0.80 |
| Er | 1.03 | 0.50 | 0.86 | 0.58 | 0.74 | 0.25 | 2.90 | 2.30 |
| Tm | 0.17 | 0.09 | 0.14 | 0.10 | 0.13 | 0.04 | 0.40 | 0.33 |
| Yb | 1.17 | 0.59 | 0.82 | 0.76 | 0.84 | 0.03 | 2.80 | 2.20 |
| Lu | 0.21 | 0.10 | 0.12 | 0.13 | 0.14 | 0.04 | 0.43 | 0.32 |
| LREE | 90.20 | 23.45 | 84.69 | 34.54 | 58.22 | 2.49 | 165.60 | 132.48 |
| HREE | 7.95 | 3.45 | 5.46 | 3.66 | 5.13 | 1.18 | 17.40 | 13.89 |
| LREE/HREE | 11.35 | 6.79 | 15.52 | 9.45 | 11.35 | 2.11 | 9.52 | 9.54 |
| ∑REE | 98.15 | 26.91 | 90.15 | 38.20 | 63.35 | 3.67 | 183.00 | 146.37 |
| GdN/YbN | 0.21 | 0.13 | 0.17 | 0.10 | 0.15 | 0.14 | 0.14 | 0.13 |
| LaN/SmN | 3.50 | 6.30 | 5.72 | 4.40 | 4.98 | 5.35 | 5.11 | 4.96 |
| LaN/LuN | 9.67 | 5.17 | 12.25 | 7.00 | 8.52 | 8.24 | 9.00 | 8.19 |
| Eu/Eu* | 0.77 | 0.52 | 0.49 | 0.69 | 0.62 | 0.58 | 0.59 | 0.62 |
| Ce/Ce* | 0.91 | 1.52 | 1.88 | 0.87 | 1.29 | 1.39 | 1.36 | 1.23 |

**Provenance:**

In order to determine the source of sediments using trace–elements (for example, Th, Co, Ni, Sc, Zr, Hf and Nb), it is necessary to ascertain that the element is relatively immobile in the sedimentary cycle **(Bhatia and Crook, 1986; McLennan, 2001; Shao *et al.*, 2001)**. Th abundances are higher in felsic than in mafic igneous source rocks and in their weathered products, whereas Co, Sc and Cr are more concentrated in mafic than felsic igneous rocks and in their weathered products. Mafic and felsic source rocks differ significantly in the ratios such of La/Sc, Th/Sc, La/Co, Th/Co and Cr/Th and hence provide useful information about the provenance of sedimentary rocks **(e.g., Cullers *et al.*, 1988; Cullers, 2000; Cullers and Podkovyrov, 2000)**. In this study, La/Sc, Th/Sc, La/Co and Th/Co values of the quartzites are more similar to values for sediments derived from felsic source rocks than to those for mafic source rocks, thus suggesting felsic source rock (Table 8).

**Table 8:** Range of elemental ratios from quartzites samples of the study area compared to elemental ratios derived from felsic rocks, mafic rocks and Upper continental crust

| Elemental Ratio | Upper continental crust[2] | Range of sediments from mafic sources[1] | Range of sediments from felsic sources[1] | Range of quartzites from study area |
|---|---|---|---|---|
| La/Sc | 2.21 | 0.43-086 | 2.50-16.3 | 2.77 |
| Th/Sc | 0.79 | 0.05-0.22 | 0.84-20.5 | 1.01 |
| La/Co | 1.76 | 0.14-0.38 | 1.80-13.8 | 4.25 |
| Th/Co | 0.63 | 0.04-1.40 | 0.67-19.4 | 1.68 |
| Cr/Th | 7.76 | 25-500 | 4.00-15.00 | 9.16 |

1.Cullers;2000), Cullers and Podkovyrov(2000); Cullers et al. (1988); 2. McLennan (2001), Taylor and McLennan (1985)

Th/Sc ratio commonly reflects the average composition of the source rocks. Scandium and Th are transferred quantitatively from source to sediment; hence, the ratio is used to deduce the composition of the source rock **(McLennan *et al.*, 1993)**. Enrichment of zircon, and therefore recycling and sorting, can be inferred from the Th/Sc versus Zr/Sc diagram; the ratio Zr/Sc is an effective index of zircon enrichment while the ratio Th/Sc is a good indicator of igneous chemical differentiation processes **(McLennan et al., 1993)**. When Th/Sc is plotted on the diagram of Zr/Sc–Th/Sc (Fig. 10) the recycled source rocks for the all-quartzite samples from the study area are further supported by their high Zr/Sc ratio. Strongly enriched Zr in zircon can be easily recycled and Sc is present in labile phases. Therefore, the Zr/Sc ratio is considered as one of the proxy to evaluate the presence or absence of recycling **(McLennan *et al.*, 1993)**. Out of four samples two samples are enriched in zircon due to sedimentary sorting and recycling and the rest two samples fall in between andesitic to felsic magmatism field. For the studied shale samples none of the samples plot in the high Zr/Sc field characteristic of zircon accumulation associated with sediment sorting and recycling rather it is approaching towards the Zr addition field for Zr/Sc ratio (Fig. 10). Besides, zircon, which is in heavy rare earth elements (HREE), contributes to a reduced chondrite-normalized $(La/Yb)_N$ ratio upon its accumulation. Hence, the presence of zircon in the studied shale samples would likely yield a negative correlation between Zr and $(La/Yb)_N$ which is clearly being depicted (Fig. 11) and it, therefore supports preferential zircon accumulation in the samples.

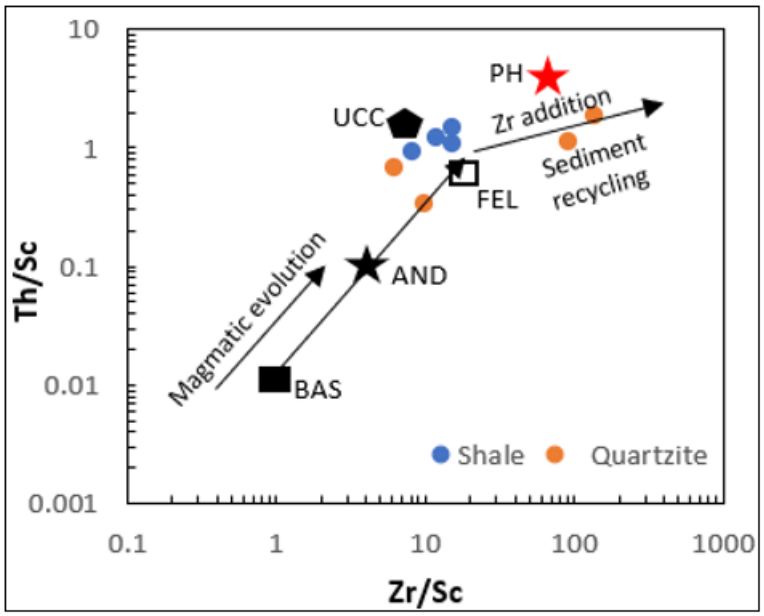


**Figure 10:** Plot of Th/Sc vs Zr/Sc of quartzite samples from study area (modified after McLennan et al.,1993) Legend: PHG=Phanerozoic granite; FEL=felsic volcanic rock; AND= andesite; BAS=basalt (igneous rock averages from Condie,1993); UCC=Upper continental crust (composition from Taylor and McLennan,1985). The lower and intermediate arrows (compositional trend) define the trend expected in first cycle sediments due to magmatic evolution from mafic to felsic; upper arrow shows the trend produced by the addition of zircon during sedimentary sorting and recycling.

The composition of major element or oxides in shales and quartzites has also been used to determine sedimentary provenance by the application of discriminant function analysis **(Murali,1983)**. This discriminant function analysis distinguishes between four major provenance fields, namely, mafic igneous, intermediate igneous, felsic igneous and quartzose sedimentary or recycled. All the studied shale and quartzite samples falls in the quartzose sedimentary provenance field (Fig. 12).

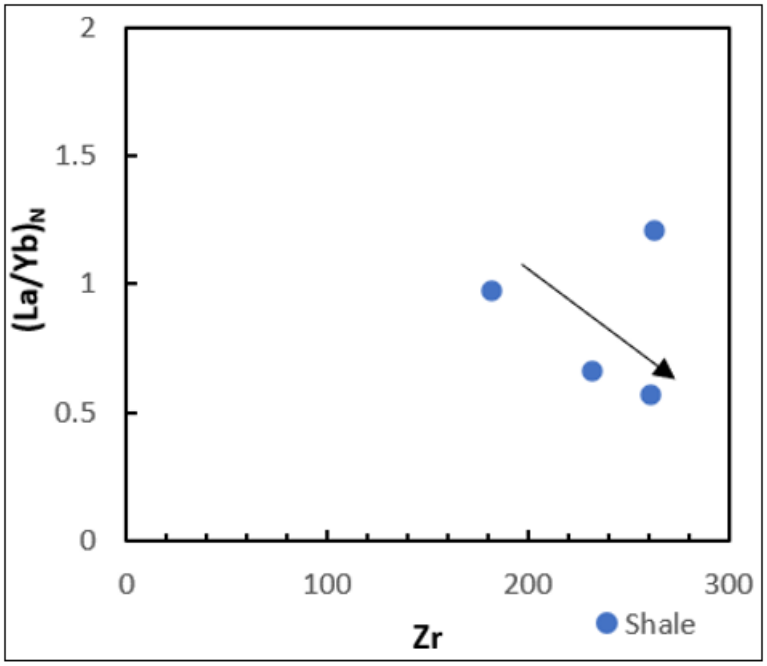


**Figure 11:** Plot of (La/Yb)N versus Zr for the studied shales of Cumbum Formation.

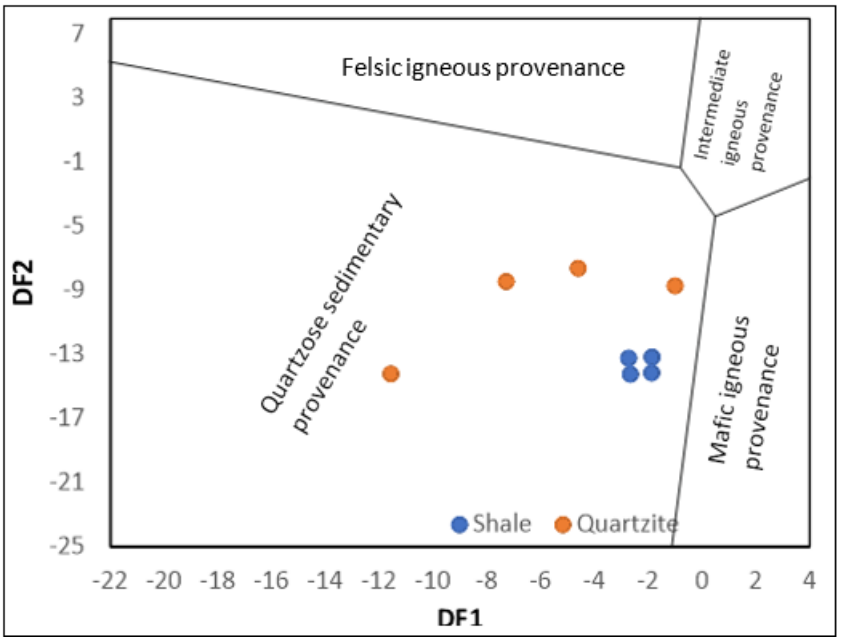


**Figure 12:** Major element Discriminant Function diagram for the shales and quartzite samples (after Murali, 1983). The discriminant functions are: Discriminant Function 1 = (−1.773 TiO2) + (0.607 Al2O3) + (0.760 Fe2O3) + (−1.500 MgO) + (0.616 CaO) + (0.509 Na2O) + (−1.224 K2O) + (−9.090); Discriminant Function 2 = (0.445 TiO2) + (0.070 Al2O3) + (−0.250 Fe2O3) + (−1.142 MgO) + (0.438 CaO) + (1.475 Na2O) + (−1.426 K2O) + (-6.861).

The binary plot of $TiO_2$ versus Zr shows that all the shale and sandstone samples are from felsic igneous rocks (Fig. 13a). Further, $TiO_2$-Ni diagram (after Floyd et al., 1989) indicates that the primary origin of the majority of samples is predominantly acidic magmatic in nature (Fig. 13b) though the shale samples fall in the extension of acidic magmatic field. The bivariate plot of La/Th against Hf (Fig. 14) and ternary diagram of V-Ni-Th*10 (Fig. 15) indicates that the studied quartzites and shales are derived from felsic source rocks.

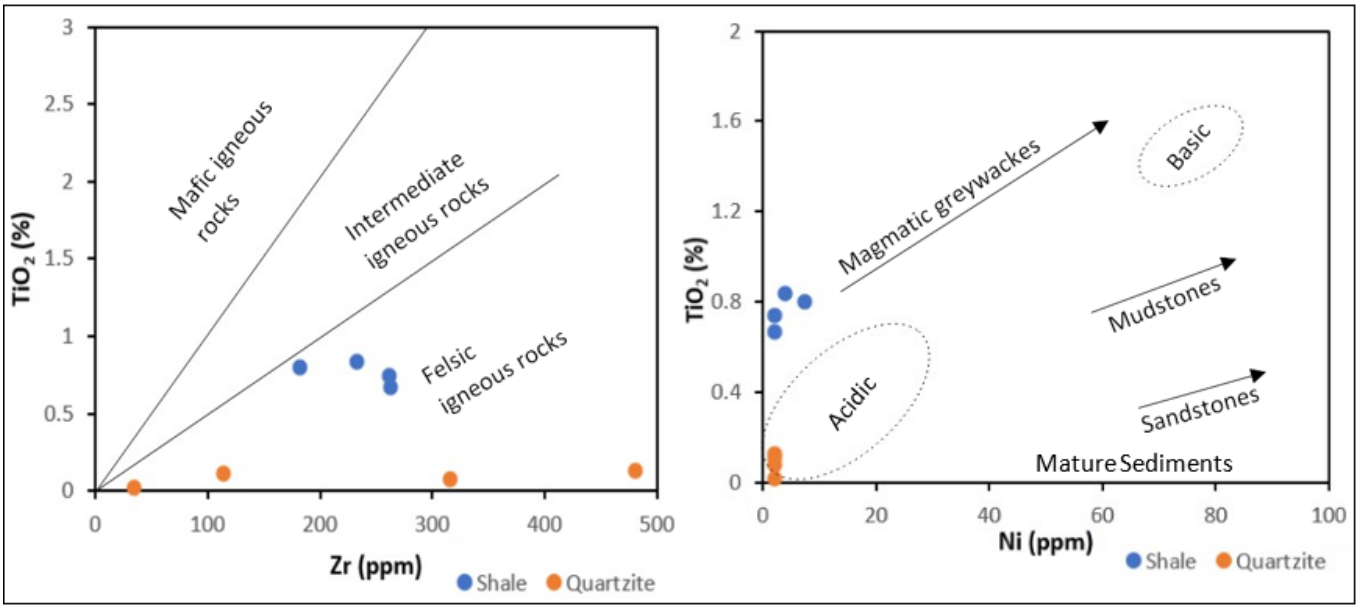


**Figure 13:** (A) $TiO_2$–Zr plot of shales and quartzites samples from the Cumbum Formation (after Hayashi et al., 1997). (B) $TiO_2$ vs Ni bivariate plot for shales and quartzite samples from the Cumbum Formation (after Floyd et al. 1993)

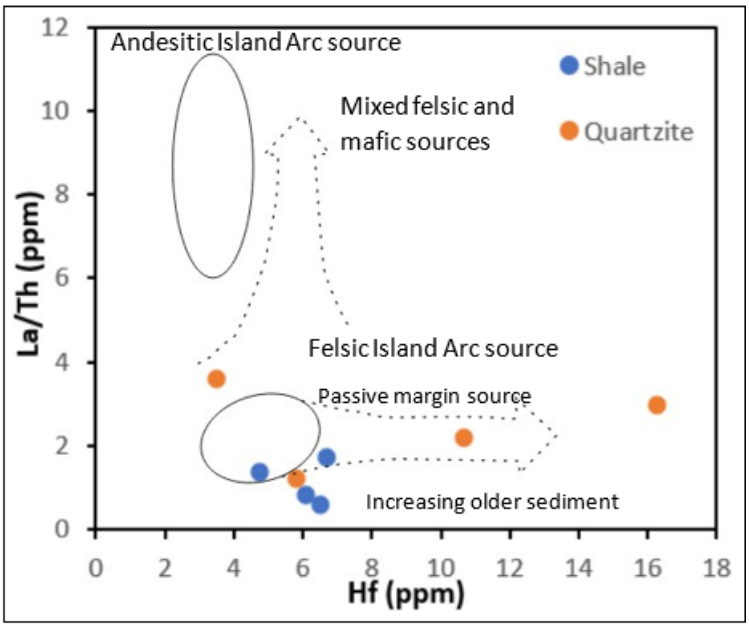


**Figure 14:** Hf vs La/Th plot for the shales and quartzites of Cumbum Formation (Floyd and Leveridge, 1987).

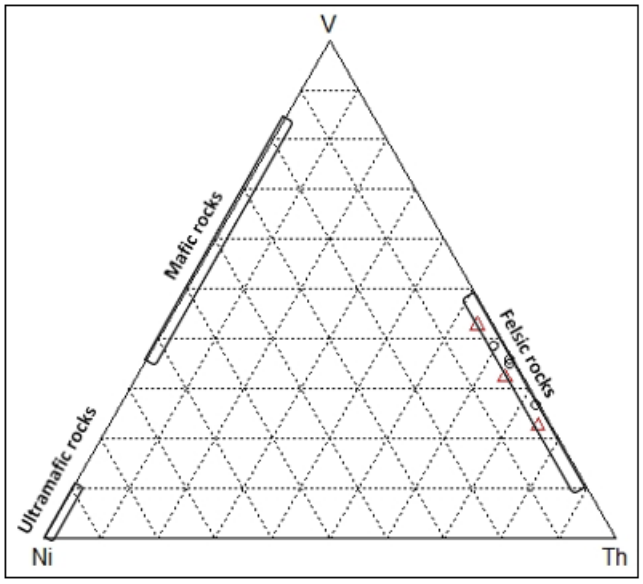


**Figure 15:** V-Ni-Th*10 triangular diagram for the Cumbum shales and quartzites **(after Bracciali et al., 2007)**. Rectangular area represents composition of the felsic, mafic, and ultramafic rocks.

**Weathering and Diagenesis of source area:**

The intensity of chemical weathering on source rocks primarily depends on factors such as the composition of the source rock, the duration of weathering, prevailing climatic conditions, and the rates of tectonic uplift in the source region **(Wronkiewicz, D.J., Condie, K.C., 1987)**. Upper crust composed mostly of feldspars and volcanic glass undergoes chemical weathering to form clay minerals. During chemical weathering, Ca, Na and K are largely removed from source rocks and the amount of these elements surviving sedimentation derived from the rocks served as indicator of the intensity of chemical weathering **(Nesbitt et al, 1997)**. For most rocks, Rb to Sr ratio increases as chemical weathering progresses. This occurs because Rb+, a relatively large alkali trace element, tends to remain concentrated in the weathered residue, while the smaller Sr2+ is preferentially leached out **(McLennan et al., 1993; Nesbitt et al., 1980)**. Consequently, the Rb/Sr ratio serves as a tool for assessing the degree of chemical weathering in the source area; an Rb/Sr ratio greater than 1 indicates a high degree of chemical weathering, whereas a ratio less than 1 suggests moderate to low levels of chemical weathering. The studied shales exhibit Rb/Sr ratios ranging from 5.24 to 13.57 (with an average of 7.87), indicating a high degree of chemical weathering in the sediment source area. Th/U in sedimentary rocks is of interest, as weathering and recycling typically result in loss of U, leading to an elevation in the Th/U ratio. The Th/U ratio in most upper crustal rocks is typically between 3.5 and 4 and Th/U values higher than 4 may indicate intense weathering in source areas or sediment recycling **(McLennan *et al.*, 1993)**. Th/U ratios in the quartzites from study area range from 0.83 to 1.45 indicating the quartzites neither suffered intense weathering nor intense recycling. But the Th/U values in the studied shales range from 4.00 to 5.76 (average 5.21) which is well above upper crustal values, and the U concentrations range from 3.48 to 5.31 ppm (average 4.43 ppm) well above that of typical shales (U ~ 3.1) and upper continental crust (U ~ 2.7) **(Taylor & McLennan, 1985)**. This suggests a high degree of chemical weathering at the sediment source area.

To quantify the extent of chemical weathering undergone by the rocks of the provenance area of clastic sediments, Nesbitt and Young (1984) introduced a parameter called the chemical index of alteration CIA to be calculated from the molecular proportions of oxides (Al, Ca, Na and K) from chemical analyses (in wt.%) of soils and sediments. This index is defined as;

$CIA=(Al_2O_3)/(Al_2O_3+CaO^*+Na_2O+K_2O)*100$ represents the Ca in silicate fraction only.

Soils and sediments derived from intensely weathered rocks and containing residual clay minerals such as kaolinite and or gibbsite have CIA values approaching 100, and unweathered upper crustal rocks has a CIA value of 50 (Fedo et al., 1995). Average shale has a CIA value of about 70 to 75. Shale samples from the study area have CIA values of 80

which is well-above those of shales 70–75. The molecular proportions of $Al_2O_3$, $CaO+Na_2O$ and $K_2O$; and $Al_2O_3$, $CaO+Na_2O+K_2O$ and FeO + MgO are plotted on triangular plots separately (Nesbitt and Young, 1984, 1989) (Fig. 16). The samples plot on the two triangular diagrams in the relatively more weathered region and in the A–CN–K diagram above the granodiorite and shale (Fig. 17). These chemical characteristics of samples from shale lithounit indicate that they were formed from a source which had suffered relatively a high degree of chemical weathering. The dominance of illite and muscovite in the clay fraction of the samples supports this inference on the source of these sediments. The sediments themselves have been subjected to intense weathering subsequent to their deposition. Besides, chemical index of weathering (CIW) also provides information on the intensity of chemical weathering. In comparison to other weathering indices, the CIW is a robust method involving restricted number of components that are well-known with consistent geochemical behaviour during weathering. The CIW formula as expressed by (Harnois, L., 1988) is shown below:

$$CIW = [\ Al_2O_3 / (Al_2O_3 + CaO^* + Na_2O)] \times 100.$$

The CIW values of the studied quartzite and shale samples range from 70.96 to 94.81 (averaging 87.28) and 98.13 to 98.37 (averaging 98.23) respectively. These CIW values point to highly intensive chemical weathering.

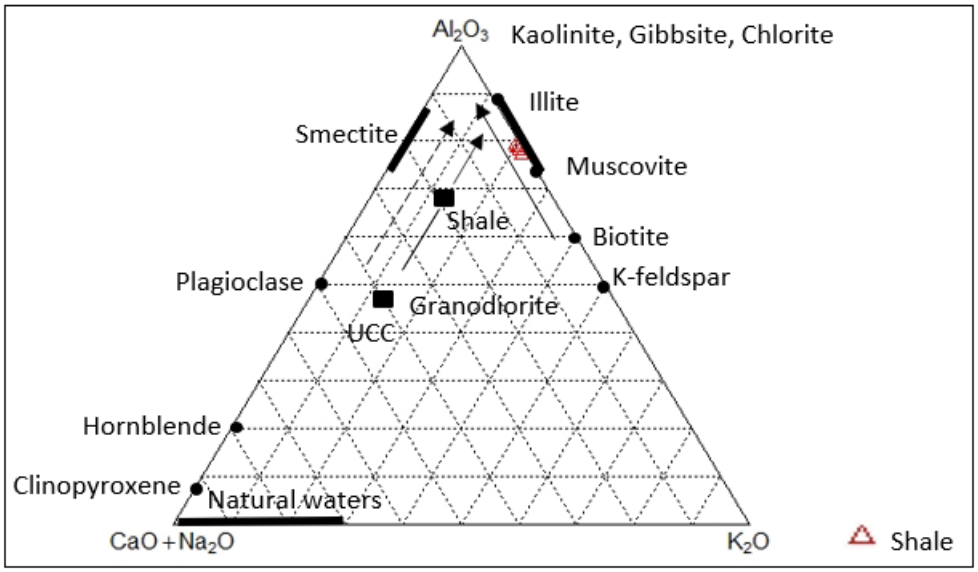


**Figure 16:** Ternary plots of A–CN–K after Nesbitt and Young 1984, 1989. A, CN, and K denote molecular proportions of $Al_2O_3$, $CaO+Na_2O$ and $K_2O$ respectively. All the plots of minerals and rocks are taken from McLennan 1995. Arrows indicate weathering trends of samples from shale lithounit plot in the region of relatively weathered material.

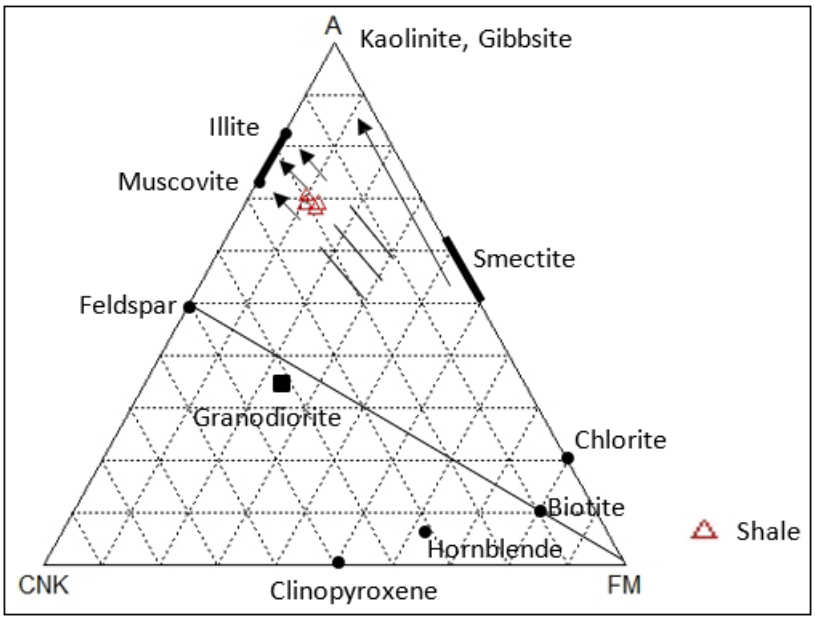


**Figure 17:** Ternary plots of A–CNK–FM after Nesbitt and Young 1984, 1989. A, CNK and FM denote molecular proportions of Al2O3, CaO+ Na2O+ K2O and FeO + MgO. All the plots of minerals and rocks are taken from McLennan 1995.

Source area weathering and elemental redistribution during diagenesis can be assessed using the plagioclase index of

alteration (PIA) **(Fedo et al, 1995)**. The maximum value of PIA is 100 for completely altered materials (i.e. kaolinite and gibbsite) and weathered plagioclase has PIA value of 50 The CIW formula as expressed by **(Fedo et al, 1995)** is shown below:

$$PIA = [(Al_2O_3 – K_2O)/ (Al_2O_3 + CaO^* + Na_2O\text{-}K_2O)] \times 100.$$

The studied shales have a range of PIA values from 68.80 to 97.55 (average, 88.34) suggesting moderate to intense weathering in the source area of the sediments.

**Climatic Conditions and Sediment Maturity:**

The prevailed climatic conditions as well as original character and maturity of sediments can be determined by calculating the index compositional variation (ICV) proposed by **(Cox et al, 1995)**. The ICV is highest for minerals that are high in weathering intensity and decreases in more stable minerals (less weathered minerals). The ICV decreases further in the montmorillonite group clay minerals and lowest in the kaolinite group minerals **(Cox et al, 1995)**. Besides, more mature shale tends to have low ICV values (< 1.0).

$$ICV = (Fe_2O_3 + K_2O + Na_2O + CaO + MgO + MnO)/Al_2O_3$$

ICV > 1 are compositionally immature with the first cycle of sediments deposited in tectonically active settings. On the other hand, those with ICV < 1 are compositionally mature and were deposited in the tectonically quiescent or cratonic environment where sediment recycling was active. For the studied quartzite and shales, the ICV values range from 0.96 to 2.09 (averaging 1.41) and 0.39 to 0.43 (averaging 0.41) respectively. Based on the average ICV values, it can be inferred that the quartzites are compositionally immature whereas the shales are compositionally mature and deposited in the tectonically quiescent or cratonic environment. The binary plot of CIA against ICV for the studied samples (Fig 18) shows that most of the shales are geochemically mature and were derived from intensively weathered source rocks. On the other hand, quartzites are immature and undergone moderate to intense chemical weathering.

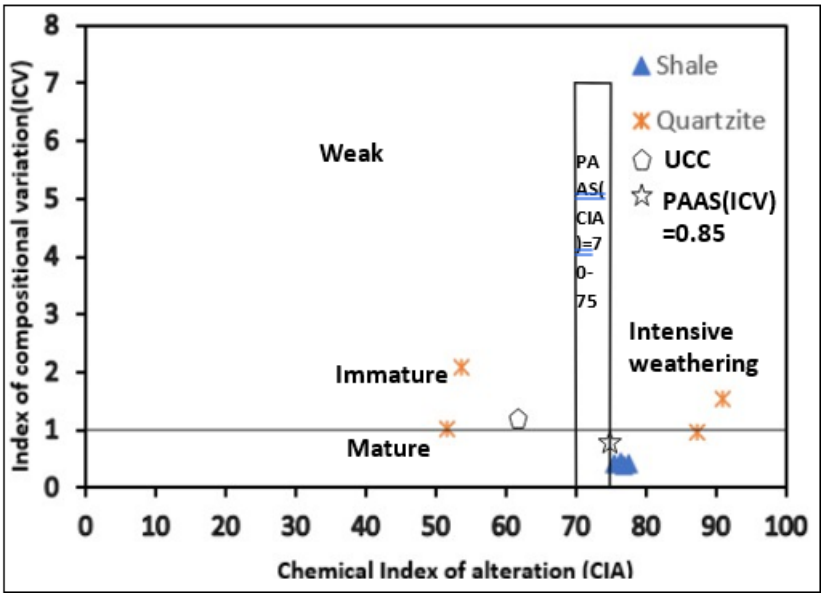


**Figure 18:** Binary plot of CIA vs ICV for the Cumbum shales and quartzites.

To assess the environmental conditions prevalent during the sedimentation of siliciclastic sedimentary rocks, a proposed diagram correlating $SiO_2$ with the sum of $Al_2O_3$, $K_2O$ and $Na_2O$ was used (**Suttner, L.J., Dutta, P.K., 1986**). This method categorizes the maturity of Cumbum quartzites and shales based on climate. As depicted in Fig. 19, the majority of quartzites plot in the semi-humid zone and shales are situated within the arid climate zone, with one sample of quartzite positioned at the boundary between arid and humid climatic zone, exhibiting varying degrees of maturity.

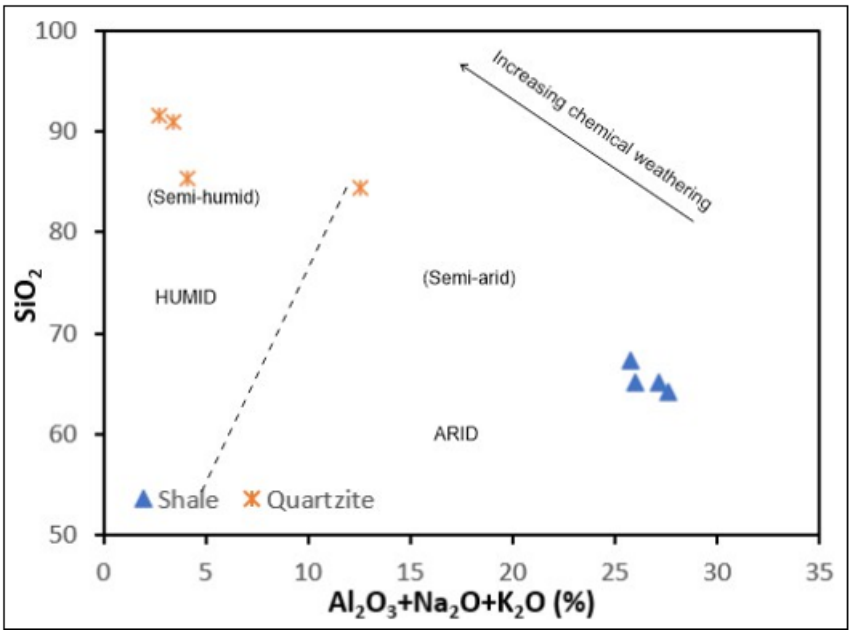


**Figure 19:** Chemical maturity for the Cumbum shales and quartzites (after Suttner, L.J., Dutta, P.K.,1986)

**Tectonic Setting and source rock characteristics:**

The chemical compositions of fine-grained siliciclastic sedimentary rocks, like shales, distinctly reflect the overall composition of their source regions and the presence of High Field Strength Elements (HFSE), transition metals and Rare Earth Elements (REEs) has been instrumental in distinguishing the source composition of these fine-grained metasedimentary rocks. **(Asiedu et al., 2017; Roddaz, Debat, & Nikiéma, 2007; Yang, Kyser, & Ansdell, 1998)**. Compared to PAAS the studied shales show enrichment in HFSE such as La, Zr, Hf, Th, Ta, and Nb, and depletion in transition metals such as Cr, Ni, Co, Sc, and V as well as LILE, suggesting a significant contribution from felsic sources (Fig 20).

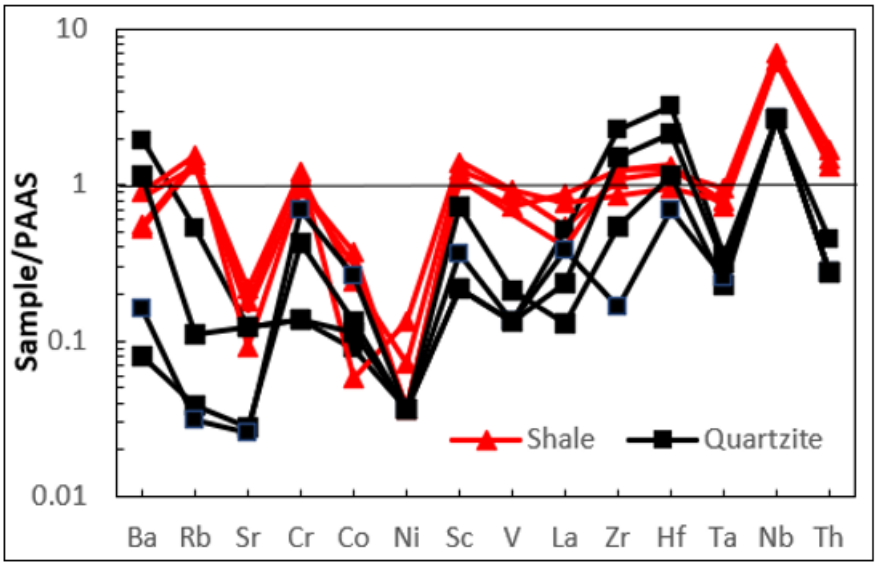


**Figure 20:** Trace element concentrations of the studied shales normalised to the composition of average PAAS. The normalising values are those of Taylor and McLennan (1985).

The systematic analysis of Co-Th-Sc-La can unveil the blending of felsic and mafic sources in sedimentary rocks **(Taylor & McLennan, 1985; Yang et al., 1998)**. In La/Sc versus Co/Th and Sc/Th versus Co/Th diagrams (Figure 21(a and b)), the investigated Cumbum shales and quartzites are positioned between felsic volcanic rock and granite end-members, predominantly clustering towards the felsic volcanic rock and TTG side (exhibiting moderate La/Sc and Co/Th). The geochemistry of the studied shales suggests they originated from a combination of felsic volcanic rocks (predominantly) and granitic rocks (to a lesser extent).

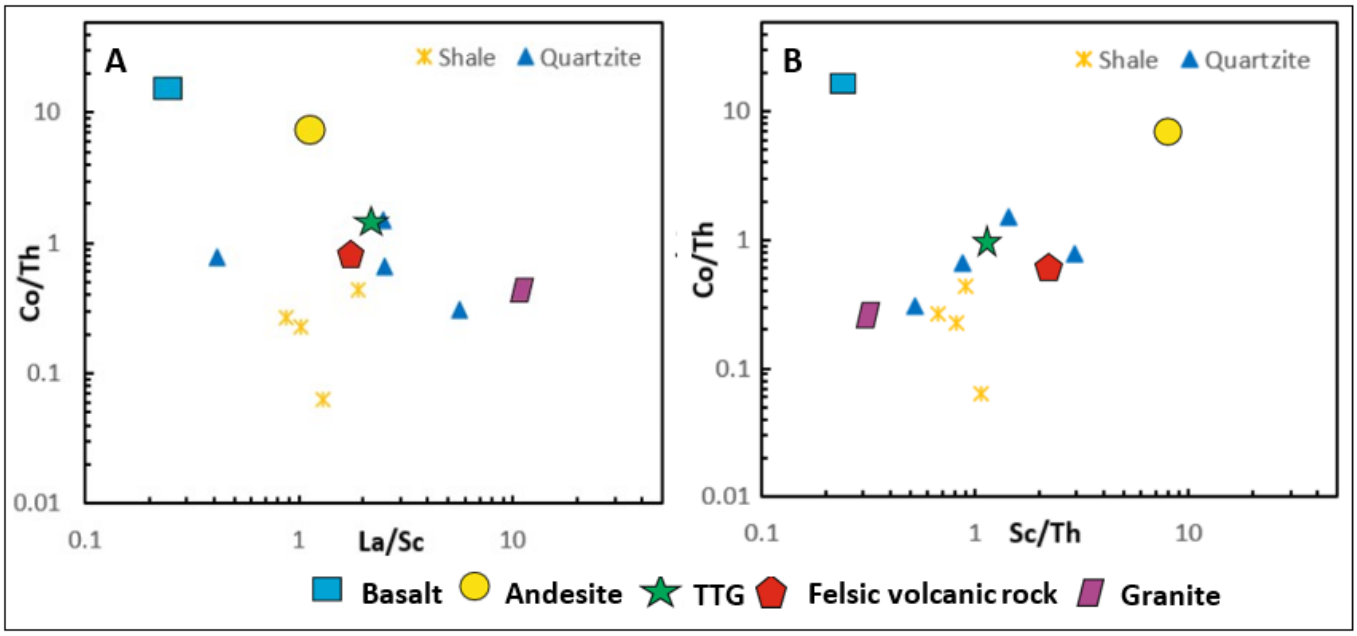


**Figure 21:** Plots of (A) Co/Th versus La/Sc and (B) Co/Th versus Sc/Th for the metasedimentary rocks of the Cumbum Formation. Also plotted are average Paleoproterozoic volcanic and plutonic rocks from Condie (1993).

The geochemical makeup of siliciclastic sedimentary rocks has been utilized to differentiate the tectonic environments of sedimentary basins, as demonstrated by studies such as those conducted by **Bhatia (1983)** and **Roser & Korsch (1986)**. Tectonic discrimination diagrams employing immobile trace elements, beneficial for Precambrian metasedimentary rocks, have proven valuable. Notably, using diagrams such as Th–Sc–Zr and Th–La–Sc, the Cumbum shales fall within passive continental margin (Fig. 22 a & b).

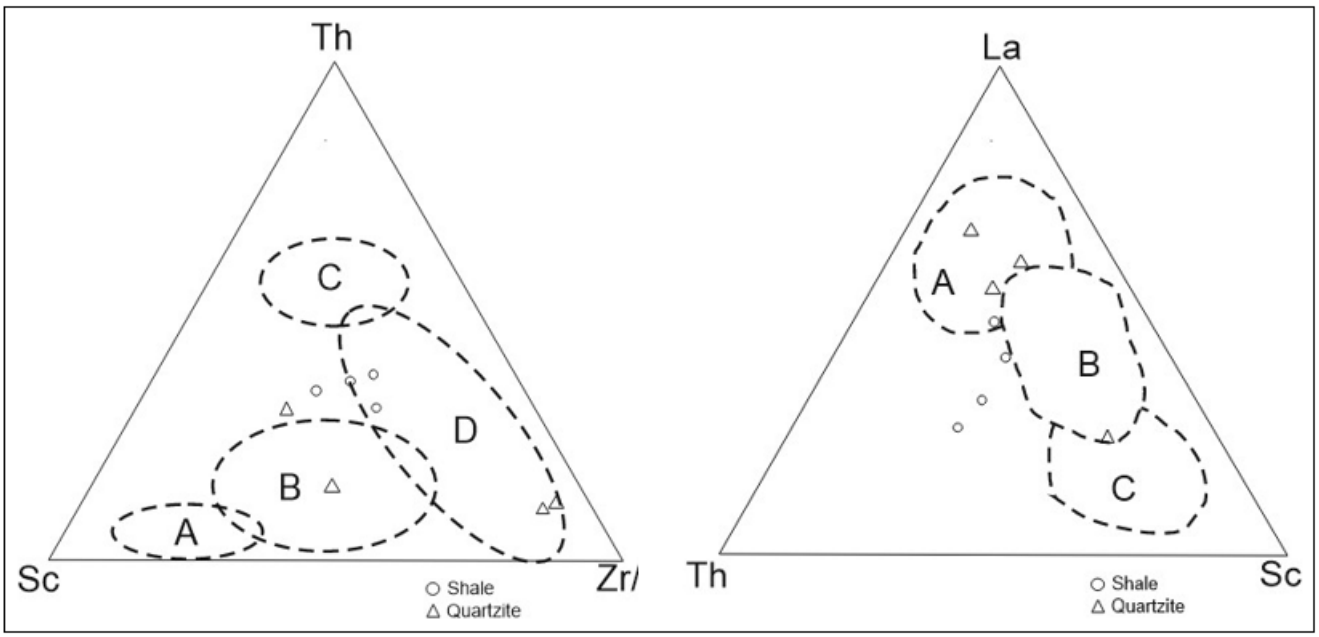


**Figure 22:** Plots of (A) Th – Co – Zr, and (B) Th – La – Sc for the tectonic setting discrimination of Cumbum shales (after Bhatia & Crook, 1986). A, Oceanic Island Arc; B, Continental Island Arc; C, Active Continental Margin; D, Passive Continental Margin.

Bivariate plots of major and trace element geochemistry have been widely used to determine the tectonic setting of quartzites and shales. Major element-based discrimination diagrams of (Bhatia and Crook, 1986) and (Bhatia, M.R.,1983) are widely used. Bhatia, 1983 has categorized a series of plots to distinguish between four primary tectonic environments: oceanic island arc (OIA), continental island arc (CIA), active continental margin (ACM), and passive continental margin (PM). Bivariate plots of $TiO_2$ versus ($Fe_2O_3$ + MgO) and $Al_2O_3/SiO_2$ against $Fe_2O_3$ + MgO indicate that the majority of the analysed samples falls in the projected extension of passive continental margin (Figures 23a and 23b).

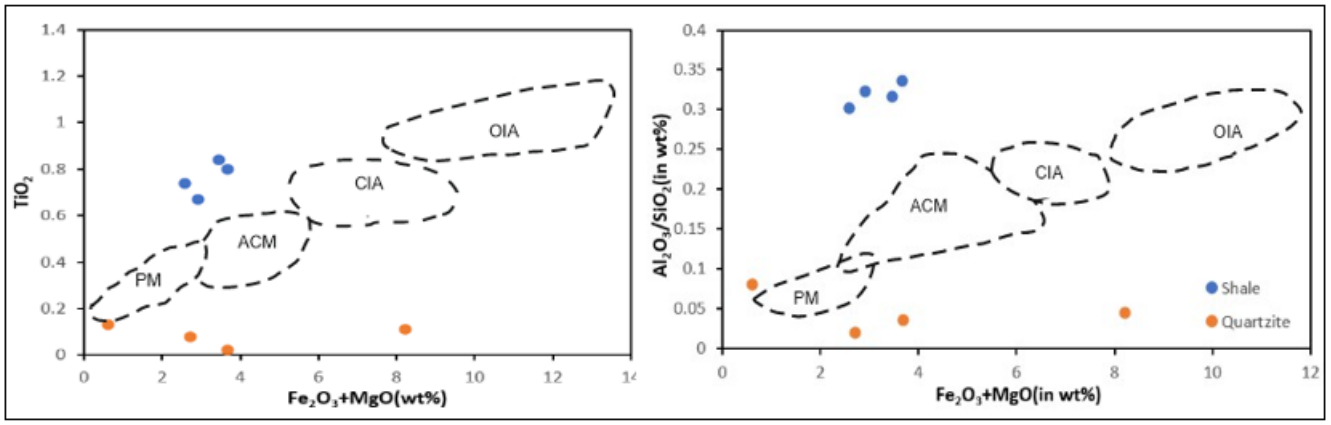


**Figure 23:** (A) Bivariate plots of (a) TiO2 (wt.%) versus (Fe2O3 + MgO) (wt.%), (b) Al2O3/SiO2 versus Fe2O3 + MgO (wt.%)

The shale and quartzite samples falls in the passive continental margin (Fig 24). Passive continental margins are basins on continental crust and basins associated with ocean floor spreading, failed rifts. Th/U ratio typically ranges from 3.5 to 4.0 for the majority of upper crustal rocks **(McLennan et al., 1993; Taylor & McLennan, 1985)**. When plotted on the Th/U versus Th diagram (Fig. 25), the analysed quartzites predominantly fall within the depleted mantle sources field, indicating a geochemically depleted mantle origin. Weathering typically results in the oxidation and subsequent dissolution of U thereby elevating the Th/U ratios above the upper crustal values, especially for shales **(Taylor & McLennan, 1985)**. The Th/U values in the studied shales range from 4 to 5.76 (average 5.21) which is well above upper crustal values, and the U concentrations range from 3.48 to 5.31 ppm (average 4.43 ppm) well above that of typical shales (U ~ 3.1) and upper continental crust (U ~ 2.7) **(Taylor & McLennan, 1985)**. This suggests a high degree of chemical weathering at the sediment source area. The above geochemical signatures, therefore, suggest the Cumbum shales are derived from older crustal material which has undergone high degree of chemical weathering.

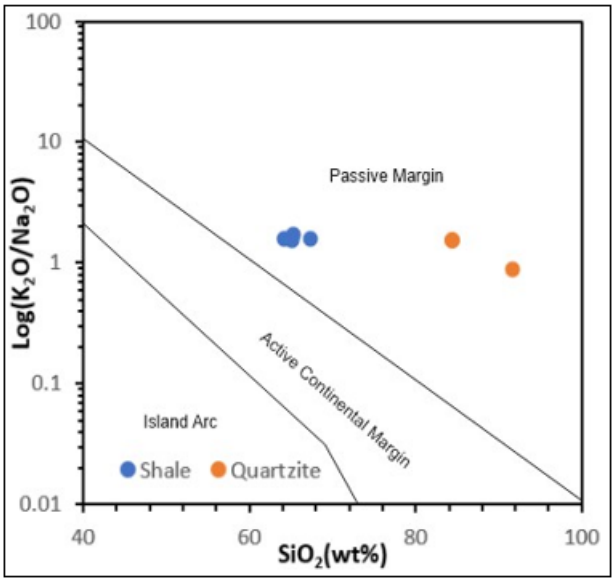


**Figure 24:** K2O/Na2O versus SiO2 tectonic-setting discrimination diagram for the Cumbum shales and quartzites.

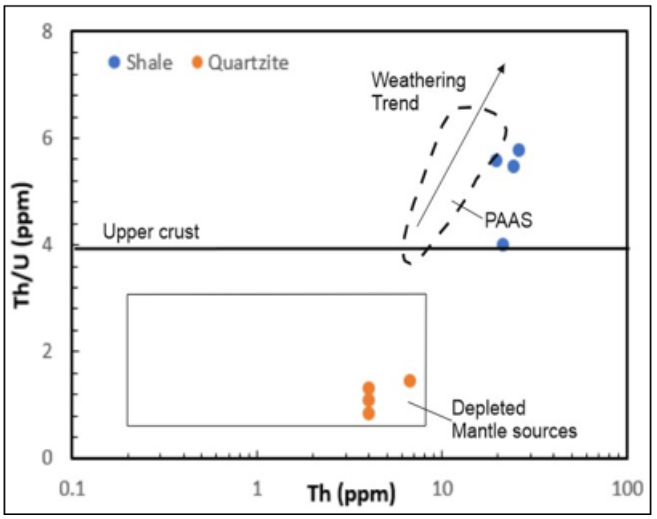


**Figure 25:** Plot of Th/U versus Th for the Cumbum shales and quartzites (after McLennan et al., 1993)

## 5. Discussion and Conclusion

Based on the discriminant function plots using major and trace elements geochemical data, it can be inferred that the quartzites and shales are mostly of quartzose sedimentary provenance, suggesting that they were derived from a cratonic interior or recycled orogen. The binary plot of TiO2 versus Ni suggests that the Cumbum quartzites are of acidic magmatic nature and the shale samples falls above the acidic magmatic field (Fig. 13b). In addition to that, the binary plots of TiO2 versus Zr (Fig. 13a), La/Th against Hf (Fig.14) and the ternary diagrams of V-Ni-Th*10 (Fig. 15) shows that the shale and quartzite samples were derived from felsic igneous rocks. Besides compared to PAAS, the studied shales show enrichment in HFSE such as La, Zr, Hf, Th, Ta, and Nb, and depletion in transition metals such as Cr, Ni, Co, Sc, and V as well as LILE, suggesting a significant contribution from felsic sources (Fig 20).

Trace elements such as La, Ce, Nd, Y, Th, Zr, Hf, Nb, Sc, Co, and Ti are valuable for distinguishing the provenance and tectonic setting of sedimentary basins due to their relative mobility during sedimentary processes **(Bhatia, M.R. and Crook, K.A.W., 1986; Rollinson, H.R., 1993)**. In the studied samples, the concentration of high field strength elements like Hf and Zr are higher in the quartzites than the

shale samples, when compared with UCC and PAAS. The ratio Zr/Sc is an effective index of zircon enrichment while the ratio Th/Sc is a good indicator of igneous chemical differentiation processes. The recycled source rocks for the all-quartzite samples from the study area are further supported by their high Zr/Sc ratio, while the presence of zircon in the studied shale samples shows a negative correlation between Zr and $(La/Yb)_N$ (Fig.10 and Fig.11). For the tectonic setting discrimination, the La/Th vs Hf (Fig.14) shows a passive margin source with increasingly older sediment. From the La/Sc versus Co/Th and Sc/Th versus Co/Th systematics, the studied shales originated from a combination of felsic volcanic rocks (predominantly) and granitic rocks (to a lesser extent) (Fig. 21a and 21b). Using diagrams such as Th–Sc–Zr and Th–La–Sc, the Cumbum shales fall within passive continental margin (Fig 22a &b). Bivariate plots of $TiO_2$ versus ($Fe_2O_3$ + MgO) and $Al_2O_3/SiO_2$ against $Fe_2O_3$ + MgO indicate that the shale samples fall in the projected extension of passive continental margin (Fig. 23a&b). Similarly, the $K_2O/Na_2O$ versus $SiO_2$ tectonic-setting discrimination diagram for the Cumbum shales and quartzites suggests the samples to be derived in a passive margin setting.

The high degree of chemical weathering for the Cumbum shales at sediment source area is depicted from the high Th/U value along with high U concentrations (Fig. 25) suggesting the shales to be derived from older crustal material.

Shale samples from the study area have CIA values of 80 which is well-above those of shales (avg. 70–75) . The molecular proportions of $Al_2O_3$, CaO+$Na_2O$ and $K_2O$ (A-CN-K) ; and $Al_2O_3$, CaO+ $Na_2O$+ $K_2O$ and FeO + MgO (A-CNK-FM) are plotted on triangular plots separately (Nesbitt and Young, 1984, 1989) (Fig. 16 and 17). The samples plot on the two triangular diagrams in the relatively more weathered region which indicates that they were formed from a source which had suffered relatively a high degree of chemical weathering and the same is inferred from the dominance of illite and muscovite in the clay fraction of the samples. The CIW values of the studied quartzite and shale samples range from 70.96 to 94.81 (averaging 87.28) and 98.13 to 98.37 (averaging 98.23) respectively suggesting high intensive chemical weathering. Here, the CIW values are higher than those of CIA due to removal of $K_2O$ from the index. The studied shales have a range of PIA values from 68.80 to 97.55 (average, 88.34) suggesting moderate to intense weathering in the source area of the sediments with the removal of feldspars during source weathering, transport, sedimentation and diagenesis. The binary plot of CIA against ICV for the studied samples (Fig 18) shows that most of the shales are geochemically mature and were derived from intensively weathered source rocks whereas the quartzites are immature and undergone moderate to intense chemical weathering. The climatic conditions for the majority of quartzites plot in the semi-humid zone whereas shales are situated within the arid climate zone, with one sample of quartzite positioned at the boundary between arid and humid climatic zone, exhibiting varying degrees of maturity.

Based on the whole-rock geochemical study on Cumbum shales and quartzites in order to deduce the provenance, tectonic setting and source area weathering. The following conclusions were made:

a) The quartzites and shales are mostly of quartzose sedimentary provenance, derived from a cratonic interior or recycled orogen. Based on the major and trace element geochemical plots, the shale and quartzite samples have contribution from felsic sources.
b) The shales and quartzites were deposited in an passive margin setting.
c) Th/U versus Th systematics suggests a high degree of chemical weathering for the Cumbum shales suggesting them to be derived from an older crustal material and a depleted mantle source for the quartzites.
d) The geochemistry of the studied shales suggests they originated from a combination of felsic volcanic rocks (predominantly) and granitic rocks (to a lesser extent).
e) The analysis of ancient weathering conditions using the chemical index of alteration (CIA), plagioclase index of alteration (PIA), and A-CN-K ($Al_2O_3$-CaO+$Na_2O$-$K_2O$) suggests that chemical weathering in the source region and recycling processes have been significant in the shales and quartzites. High CIA values, indicating high weathering intensities of the samples, and suggesting a arid-humid paleoclimate for the source area.

**Author Contributions**

RM involved in field investigation, conceptualization, methodology, software and writing of original draft. SD collected baseline data and involved in field investigation.

**Acknowledgement:**

The work has been carried out under Misiion-II Project of Geological Survey of India, State Unit: Andhra Pradesh, SR, Hyderabad during field season programme 2020-21. The authors are grateful to Director General, Geological Survey of India, Addl. Director general, Geological Survey of India, Southern Region, Hyderabad and Shri R.P. Nagar, Dy. Director General, State Unit: Andhra Pradesh, Southern Region, Hyderabad for providing necessary facilities and support to carry out the work.

**Declaration of interest:** The authors declared that there is no any actual or potential conflict of interest including any financial, personal or other relationships with other people or organizations regarding the publication of this original manuscript.

## References

[1] Asiedu, D.K., Asong, S., Atta-Peters, D., Sakyi, P.A., Su, B.X., Dampare, S.B. and Anani, C.Y. (2017) Geochemical and Nd-Isotopic Compositions of Juvenile-Type Paleoproterozoic Birimian Sedimentary Rocks from Southeastern West African Craton (Ghana): Constraints on Provenance and Tectonic Setting. Precambrian Research, 300, 40-52.

[2] Bauluz, B., Mayayo, M.J., Fernandez-Nieto, C. and Lopez, J.M.G. (2000) Geochemistry of Precambrian and Paleozoic siliciclastic rocks from the Iberian Range (NE Spain): implications for source-area weathering, sorting, provenance, and tectonic setting. *Chemical Geology*, *168*(1-2), pp.135-150.

[3] Bhatia, M. R. (1983) Plate tectonics and geochemical composition of sandstones. Journal of Geology, 92, 181–193.
[4] Bhatia, M. R., and Crook, A. W. (1986) Trace element characteristics of greywackes and tectonic setting discrimination of sedimentary basins. *Contribution to Mineralogy and Petrology, 92, 181–193.*
[5] Blatt, H. G., Middleton, G. V., and Murray, R. C. (1980) Origin of sedimentary rocks (2nd ed.). Englewood cliff, N. J., Prentice Hall.
[6] Borges, J.B., Huh, Y., Moon, S. and Noh, H. (2008) Provenance and weathering control on river bed sediments of the eastern Tibetan Plateau and the Russian Far East, *Chemical Geology*, *254*(1-2), pp.52-72.
[7] Bracciali, L., Marroni, M., Pandolfi, L., Rocchi, S. (2007) Geochemistry and petrography of Western Tethys Cretaceous sedimentary covers (Corsica and Northern Apennines): From source area to configuration of margins, in Arribas, J., Critlli, S., Johanson, M.J., (eds.), Sedimentary provenance and petrogenesis: Perspectives from petrography and geochemistry. Geological Society of America, Special Paper, 420, 73-93.
[8] Chakrabarti, G., Shome, D., Reddy, Chandra Sekhar L. and Sinha, S. (2016) Provenance and Tectonic Setting of Sedimentary Rocks of the Cuddapah basin, South India, *Research Journal of Chemical Sciences*, Vol. *6*(10), pp.1-7.
[9] Condie, K.C. (1993) Chemical composition and evolution of the upper continental crust: contrasting results from surface samples and shales, *Chemical geology*, *104*(1-4), pp.1-37.
[10] Cox, R., Low, D.R. and Cullers, R.L. (1995) The influence of sediment recycling and basement composition on evolution of mudrock chemistry in the southwestern United States, Geochimica et Cosmochimica Acta, 59, 2919-2940.
[11] Crook, K.A. (1974) Lithogenesis and geotectonics: the significance of compositional variation in flysch arenites (graywackes).
[12] Cullers, R.L. and Podkovyrov, V.N. (2000) Geochemistry of the Mesoproterozoic Lakhanda shales in southeastern Yakutia, Russia: implications for mineralogical and provenance control, and recycling., *Precambrian Research*, *104*(1-2), pp.77-93.
[13] Cullers, R.L. (2000) The geochemistry of shales, siltstones, and sandstones of Pennsylvanian-Permian age, Colorado, USA: implications for provenance and metamorphic studies. *Lithos 51, 181–203.*
[14] Cullers. R.L. (1988) Mineralogical and chemical changes of soil and stream sediment formed by intense weathering of the Danberg granite, Georgia, USA. *Lithos 21, 301–314.*
[15] Das, B. K., Al- Mikhlafi. A.S. and Kaur, P. (2006) Geochemistry of Mansar Lake sediments, Jammu, India: Implication for source-area weathering, provenance, and tectonic setting. *Journal of Asian earth sciences 26 (6) :649-668.*
[16] Fedo, C. M., Nesbitt, H. W., and Young, G. (1995) Unraveling the effects of potassium metasomatism in sedimentary rocks and palaeosols, with implications for palaeo-weathering conditions and provenance. Journal of Geology, 23, 921–924.
[17] Fedo, C.M., Eriksson, K.A. and Krogstad, E.J. (1996) Geochemistry of shales from the Archean (~ 3.0 Ga) Buhwa Greenstone Belt, Zimbabwe: implications for provenance and source-area weathering, *Geochimica et Cosmochimica Acta*, *60*(10), pp.1751-1763.
[18] Floyd, P.A. and Leveridge, B.E. (1987) Tectonic environment of the Devonian Gramscatho basin, south Cornwall: Framework mode and geochemical evidence from turbiditic sandstone, Journal of the Geological Society London, 1987, 144, 531-542.
[19] Floyd. P.A., Winchester. J.A. and Park. R.G. (1989) Geochemistry and tectonic setting of Lewisian clastic metasediments from the Early Proterozoic Loch Maree Group of Gairloch, N.W. Scotland, *Precambrian Research, 1989, 45 (1-3), 203-214.*
[20] Gromet, L.P., Haskin, L.A., Korotev, R.L. and Dymek, R.F. (1984) The "North American shale composite": Its compilation, major and trace element characteristics, *Geochimica et cosmochimica acta*, *48*(12), pp.2469-2482.
[21] Harnois, L. (1988) The CIW index: A new chemical index of weathering. Sedimentary Geology,55(3-4), 319-322.
[22] Hayashi, K.I., Fujisawa, H., Holland, H.D. and Ohmoto, H. (1997) Geochemistry of~
[23] 1.9 Ga sedimentary rocks from northeastern Labrador, Canada, *Geochimica et cosmochimica acta*, *61*(19), pp.4115-4137.
[24] Herron, M.M. (1988) Geochemical classification of terrigenous sands and shales from core or log data, *Journal of Sedimentary Research*, *58*(5), pp.820-829.
[25] Hossain, H.M.Z., Roser, B.P. and Kimura, J.I. (2010) Petrography and whole-rock geochemistry of the Tertiary Sylhet succession, northeastern Bengal Basin, Bangladesh: Provenance and source area weathering, *Sedimentary Geology*, *228*(3-4), pp.171-183.
[26] Kale, V. (1991) Constraints on the evolution of the Purana basins of peninsular India, Journal of the Geological Society of India, 38, 231–252.
[27] Lakshminarayana, G., Bhattacharjee, S. and Kumar, A. (1999) Palaeocurrents and depositional setting in the Banganapalle Formation, Kurnool sub-basin, Cuddapah basin, Andhra Pradesh, *Journal-geological society of India*, *53*, pp.255-260.
[28] Levinson, A.A. (1974) Introduction to Exploration Geochemistry, Applied Publication Limited, Calgary, p. 1965.
[29] Madhavaraju, J. and Lee, Y.I. (2010) Influence of Deccan volcanism in the sedimentary rocks of Late Maastrichtian–Danian age of Cauvery basin Southeastern India: constraints from geochemistry, *Current Science*, pp.528-537.
[30] Matin, A. (2015) Chapter 16 Tectonics of the Cuddapah Basin and a model of its evolution: a review. *Geological Society London, Memoirs*, *43*(1), pp.231-254.
[31] McLennan, S. M. (2001) Relationships between the trace element composition of sedimentary rocks and upper continental crust, *Geochem. Geophys. Geosys. 2 (article no. 2000GC000109).*
[32] McLennan, S.M. (1989) Rare Earth Elements in Sedimentary Rocks: Influence of Provenance and

Sedimentary Process, Review of Mineralogy, 21, 169-200.

[33] McLennan, S.M., Hemming, S. and McDanei, D.K. (1993) Geochemical Approaches to Sedimentation, Provenance and Tectonics, In: Johnsson, M.J. and Basu, A., Eds., Processes Controlling the Composition of Clastic Sediments: Geological Society of America, Special Papers, 285, 21-40.

[34] Meijerink, A.M.J., Rao, D.P. and Rupke, J. (1984) Stratigraphic and structural development of the Precambrian Cuddapah basin, S.E. India, *Precambrian Research*, 26(1), pp. 57–104.

[35] Mishra, R. and Dash, S. (2021) Reconnaissance survey for barytes in the southern extension of the Mangampeta barite deposit, Kadapa District, Andhra Pradesh *Unpublished GSI Report* (FS 2020-01).

[36] Murali, A.V., Parthasarathy, R., Mahadevan, T. M. and Das, S. M. (1983) Trace element characteristics, REE patterns and partition coefficients of zircons from different geological environments: A case study on Indian zircons. *Geochimica et Cosmochimica Acta, 1983, 47, 2047-2052.*

[37] Nesbitt, H. W. and Young, G. M. (1984) Prediction of some weathering trends of plutonic and volcanic rocks based on thermodynamic and kinetic considerations, Geochimica Cosmochimica Acta, 48, 1523–1534.

[38] Nesbitt, H. W., Markovics, G. and Price, R. C. (1980) Chemical processes affecting alkalis and alkaline earths during continental weathering, Geochimica et Cosmochimica Acta, 44, 1659–1666.

[39] Nesbitt, H.W., Fedo, C.M. and Young, G.M. (1991) Quartz and feldspar stability, steady and non-steady state weathering and petrogenesis of siliciclastic sands and muds, Journal of Geology, 1997, 105, 173-191.

[40] Nesbitt, H.W. and Young, G.M. (1989) Formation and diagenesis of weathering profiles, Journal of Geology, 1989, 97, 129-147.

[41] Pettijohn, F.J., Potter, P.E. and Siever, R. (1972) Production and provenance of sand. *Sand and Sandstone*, pp.294-326.

[42] Rao, Nagaraja B. K., Rajurkar, S. T., Ramlingaswamy, G. and Babu, B. R. (1987) Stratigraphy, Structure and Evolution of the Cuddapah Basin, Memoir Geological Society of India, Vol. 6, pp. 33-87.

[43] Rao, N. and Ramalingaswamy. B.K. (1976) Some new thoughts on the stratigraphy of Cuddapah Supergroup – Badami, Bhima and Cuddapah Supergroup, Mysore, 17-20 abstracts.

[44] Rao, N., Ramalingaswamy, B.K., Rajurkar, G. and Ravindra Babu, B. (1987) Stratigraphy, structure and evolution of the Cuddapah basin In: Purana basins of Peninsular India (Middle to Late Proterozoic) *Geological Society of India Memoirs*, 6: 33-86.

[45] Roddaz, M., Debat, P., and Nikiéma, S. (2007) Geochemistry of Upper Birimian sediments (major and trace elements and Nd–Sr isotopes) and implications for weathering and tectonic setting of the Late Paleoproterozoic crust, Precambrian Research, 159, 197–211.

[46] Rollinson, H.R. (1993) Using geochemical data: evaluation, presentation, interpretation, Essex. Longman Scientific Technical, 1993, 344pp.

[47] Roser, B. P. and Korsch, R. J. (1986) Determination of tectonic setting of sandstone–Mudstone suites using SiO2 content and K2O Na2O ratio, Journal of Geology, 94, 635–650.

[48] Rudnick, R. L. and Gao, S. (2003) Composition of the continental crust, *Treatise of Geochemistry, 2003, 3, 1-64.*

[49] Saha, D. and Tripathy, V. (2012) Palaeoproterozoic sedimentation in the Cuddapah Basin, south India and regional tectonics: a review. In: Mazumder, R. & Saha, D. (eds) Palaeoproterozoic of India, Geological Society, London, Special Publications, 365, 161–184.

[50] Shao, B.B. and Lin. W.T. (2001) Measuring the value of Information technology in Technical efficiency with Stochastic production frontier, *Information and software technology, 43, 447-456.*

[51] Suttner, L.J. and Dutta, P.K. (1986) Alluvial sandstone composition and palaeoclimate: In Framework mineralogy, Journal of Sedimentary Petrology, 1986, 56, 329-345.

[52] Taylor, S. R. and McLennan, S. M. (1985) The Continental Crust: Its Composition and Evolution. Blackwell, Oxford.

[53] Taylor, S.R. and McLennan, S.M. (1995) The geochemical evolution of the continental crust, *Reviews of geophysics*, *33*(2), pp.241-265.

[54] **Vasundhara Project, Geological Survey of India, 1994**

[55] Wronkiewicz, D.J. and Condie, K.C. (1987) Geochemistry of Archean shales from the Witwatersrand Supergroup, South Africa: source-area weathering and provenance, *Geochimica et Cosmochimica Acta*, *51*(9), pp.2401-2416.

[56] Yang, H., Kyser, K. and Ansdell, K. (1998) Geochemical and Nd isotopic compositions of the metasedimentary rocks in the La Ronge Domain, Trans-Hudson Orogen, Canada: Implications for evolution of the domain. Precambrian Research, 92, 37–64.